

MICRO-RAMAN SPECTROSCOPY OF CARIES LESION FORMATION IN
DENTAL ENAMEL

By

DEEPA DADLANI

A thesis submitted to the

Graduate School-New Brunswick

Rutgers, The State University of New Jersey

and

The Graduate School of Biomedical Sciences

University of Medicine and Dentistry of New Jersey

in partial fulfillment of the requirements

for the degree of

Master of Science

Graduate Program in Biomedical Engineering

written under the direction of

Dr. Adrian Mann

and approved by

New Brunswick, New Jersey

January, 2008

ABSTRACT OF THE THESIS

MICRO-RAMAN SPECTROSCOPY OF CARIES LESION FORMATION IN

DENTAL ENAMEL

by DEEPA DADLANI

Thesis Director:
Dr. Adrian Mann

Caries lesions form by a complex process of chemical interactions between dental enamel and its environment. They can cause cavities and pain, and are expensive to fix. Lesions form by slow demineralization over many months, even years. It is hard to characterize *in vivo* as a result of environmental factors and remineralization by ions in the oral cavity. In this thesis the process of demineralization was carried out *in vitro* and micro-Raman spectroscopy used to investigate and characterize the lesion's chemistry.

Demineralization occurs by diffusion across the depth of the lesion of mineral ions via interstitial spaces in the dental enamel. Hydroxyl ions are initially lost by acidic attack, which increases the interstitial space. The demineralization is retarded by diffusion processes in the opposite direction, and a balance in the charges of the ions must be maintained. Having multiple ions diffusing simultaneously is termed "coupled diffusion".

A subsurface highly demineralized region is formed, but this can be remineralized.

Micro-Raman spectroscopy is a powerful tool for studying material composition by exciting chemical bonds in the sample. Using micro-Raman to characterize the chemical composition of lesions may help in developing preventative measures to stop their formation. Raman ($\lambda=785$ nm) was used to characterize lesions grown over 5, 7, 9, 11

and 14 days. The amide I peak at $\sim 1605\text{ cm}^{-1}$, which has not been observed previously, was seen in the maturing lesions. The extreme demineralization in these lesions enables the organic peaks to be seen rather than the normally stronger mineral peaks. Analysis of crystallinity shows that there is always a reduction in mineral content with distance below the enamel surface, but this becomes magnified as the lesion matures. Type B carbonate substitution for phosphate ions can also be examined with Raman. Correcting for crystallinity shows that both carbonate and phosphate ions are lost at the same rate during demineralization.

In summary, micro-Raman is an effective and relatively easy tool to use in lesion characterization. It also has the advantage that it can be used to identify changes in both the mineral and protein phases of enamel.

ACKNOWLEDGEMENTS

I wish to express my greatest appreciation to:

Dr. Adrian Mann, my advisor for this patience, guidance and encouragement in understanding and bringing forth my strong analytical skills to tackle a research problem.

To my committee:

Dr. David Shreiber, Dr. Noshir Langrana and Dr. Richard Lehman for their helpful guidance and support in this research thesis.

John Yaneiro, for being enthusiastic and charming, from whom I have learnt so much and wish to hold dear.

Dr. Beril Kavukcuoglu, who recently graduated from our lab and is a post-doc at the moment, for her constant support and guidance in creating samples preparations and experimentation with lab techniques. Dr. Kavukcuoglu also mentored me on the quantitative aspect of Raman spectral data analysis.

Milca AponteRoman, for teaching me how to use the Raman Spectrometry and just being there for me, when I needed constant support and guidance.

Syeda Huessain, who helped me guide my Numerical Analysis through thought, support and understanding.

Stuart De Deutsch, Daniel Haders, Asad Mughal and Sukanya Murali for being there and providing me with their enthusiasm in research, with whom I have shared interesting thoughts and ideas.

J.D. Sorge for providing me permission to use the Solar cell laboratory and for teaching me to use the pH meter.

Dr. Richard Lehman for his constant guidance in glass ceramics engineering and his joyous input in my research analogies. Also, Dr. Lehman guided me in the process of forming Bioglass®, at his laboratory furnaces.

Felix Quintero for helping me with obtaining chemical materials for formation of Bioglass® and helping me understand the formation of Bioglass®.

To Nuria Royo, Vamsi Rani and Mike Wininger for helping me understand my research goals and reiterating the importance of research with enthusiasm.

To Dr. Troy Shinbrot, our Graduate Program Director in guiding me throughout my graduate curriculum and encouraging me to move forward with immense guidance in honing my strengths.

To my husband and in-laws, for believing in me and providing me the insight for pursuing my career goals. I can't thank my loving husband enough for the numerous sacrifices that he made while I underwent my graduate education. He opted to study Executive MBA last year, and would graduate May 2008.

To my parents, for always encouraging me to give my best at education and to excel in a competitive environment. To my grandmother and late grandfather, who believed in me and always instilled the importance of education. To my brother, and his newlywed wife for sharing fun moments.

I'm grateful to all people who haven't been acknowledged so far, for they know that they have left my life fulfilled with enormous knowledge, wisdom and love.

TABLE OF CONTENTS

| | |
|--|-----|
| ABSTRACT OF THE THESIS | ii |
| ACKNOWLEDGEMENTS..... | iv |
| TABLE OF CONTENTS..... | vii |
| LIST OF TABLES | ix |
| LIST OF FIGURES | x |
| | |
| 1 INTRODUCTION | 1 |
| 2 STRUCTURE OF DENTAL ENAMEL | 3 |
| 2.1 Introduction..... | 3 |
| 2.1.1 Dental enamel | 6 |
| 2.1.2 Microstructure of Enamel | 8 |
| 2.1.3 Lesion Microstructure, pore and lesion zones | 10 |
| 2.1.4 Hydration Layer | 13 |
| 2.1.5 Arrested Lesions: | 14 |
| 3 MATERIALS, METHODS AND CHARACTERIZATION TECHNIQUES | 16 |
| 3.1 Selection of teeth for testing | 16 |
| 3.2 Preparation of control group teeth | 16 |
| 3.3 Preparation of teeth for growth of incipient carious lesions | 17 |
| 3.4 Formation of Bioglass..... | 18 |
| 3.5 Characterization of Caries lesion through Raman spectroscopy | 19 |

| | |
|--|----|
| 4 RESULTS | 24 |
| 4.1 Change in crystallinity across sound enamel: | 24 |
| 4.2 Change in carbonate across enamel: | 31 |
| 4.3 Changes in protein structure across enamel: | 39 |
| 5 DISCUSSION | 47 |
| 6 CONCLUSION AND FUTURE WORK | 49 |
| 7 STATEMENT OF THE PROBLEM, SPECIFIC AIMS AND SIGNIFICANCE | 51 |
| 7.1 Statement of the problem | 51 |
| 7.2 Specific aims of this investigation | 51 |
| 7.3 Significance of the problem | 52 |
| 8 REFERENCES | 53 |
| 9 APPENDICES | 56 |

LIST OF TABLES

| | |
|--|----|
| Table 4.1: Phosphate to Carbonate Variation for sound enamel and lesions of 5, 7, 9, 11 and 14 days | 36 |
| Table 4.2: Phosphate to Amide III variation for sound enamel and 5, 7, 9, 11 and 14 day lesions..... | 44 |

LIST OF FIGURES

| | |
|---|----|
| Figure 2.1: Dental anatomy..... | 4 |
| Figure 2.2: Dental arch | 7 |
| Figure 2.3: FEISEM image of dental enamel magnified to x14000 (Adapted from Breschi et al., 1999) | 9 |
| Figure 2.4: FEISEM image of dental enamel magnified to x20000 (Adapted from Breschi et al., 1999) | 9 |
| Figure 2.5 Hydration layer (Adapted from Cazalbou et al., 2004)..... | 14 |
| Figure 3.1: Picture depicting the procedure for the formation of dental lesions | 17 |
| Figure 3.2 Raman effect: UV, visible and near-IR excitation strategies. | 21 |
| Figure 4.1:Crystallinity changes for sound enamel | 25 |
| Figure 4.2: Crystallinity changes for 5 day lesion | 26 |
| Figure 4.3: Crystallinity changes for a 7 day lesion | 26 |
| Figure 4.4: Crystallinity changes for a 9 day lesion | 27 |
| Figure 4.5: Crystallinity changes for a 11 day lesion | 27 |
| Figure 4.6: Crystallinity changes for a 14 day lesion | 28 |
| Figure 4.7: TOF-SIMS maps showing content of (a) total positive ion, (b) calcium, (c) potassium, (d) sodium, (e) total negative ion, (f) POxHy, (g) fluorine, and (h) chlorine through cross-section of lesion grown for 14 days in demineralization solution in human enamel (Adapted from Dickinson et al., 2007)..... | 30 |
| Figure 4.8: Carbonate Variation in Sound enamel..... | 32 |
| Figure 4.9: Carbonate variation for a 5 day lesion..... | 32 |
| Figure 4.10: Carbonate variation for a 7 day lesion..... | 33 |

| | |
|--|----|
| Figure 4.11: Carbonate variation for a 9 day lesion..... | 33 |
| Figure 4.12: Carbonate variation for a 11 day lesion..... | 34 |
| Figure 4.13: Carbonate variation for a 14 day lesion..... | 34 |
| Figure 4.14: Raman spectrum of a dental lesion showing amide I peak at 1605 cm^{-1} , Amide III at 1305 cm^{-1} , carbonate type B at 1070 cm^{-1} , type A carbonate at 1111 cm^{-1} and CH_2 at 1450 cm^{-1} . Strong phosphate peak at 959 cm^{-1} is observed. | 41 |
| Figure 4.15: Phosphate to Amide I ratios for a 9 day lesion..... | 41 |
| Figure 4.16: Phosphate to Amide I ratios for a 11 day lesion..... | 42 |
| Figure 9.1: Polished Bioglass section 20x | 58 |
| Figure 9.2: Polished Bioglass section 50x | 58 |

CHAPTER 1

INTRODUCTION

Human dental enamel when exposed to acid attack can be demineralized which combined with mechanical wear gives rise to cavities. Cavities and tooth decay are a major concern in dentistry even though fluoride treatments have significantly reduced their incidence^{1,2}. Dental demineralization can be followed by remineralization, which is known to arrest caries formation in some cases and can be used as a preventative measure. The purpose of this investigation is to understand dental lesion formation and progression by characterizing lesions at various stages of their development using micro-Raman Spectroscopic methods. The variations in carbonate solubilities in the apatite, phosphate precipitation, C-H bonds and amide bonds (I and III) across the depth of the lesion are examined over a number of days during accelerated *in vitro* lesion formation. This understanding could be further enhanced by future studies looking at isotropic materials such as Bioglass®, polycrystalline hydroxyapatite, or any other bioceramic material that is fairly homogenous in composition.

The chapters in this thesis are described below:

Chapter 2 is the dental background describing dental structures along with the current understanding of caries lesions formation.

Chapter 3 includes describes the materials, methods and characterization techniques.

Chapter 4 is the results.

Chapter 5 is a discussion.

Chapter 6 is the conclusions.

CHAPTER 2

STRUCTURE OF DENTAL ENAMEL

2.1 Introduction

Teeth are present in the mouths of primates to aid in breaking down morsels of food during mastication. Apart from its detrimental affect on the aesthetic appearance of winning smiles and otherwise, tooth decay can be extremely painful if not treated. Caries is a major problem amongst youngsters who are fascinated by soda drinks, orange juice and other acidic food products³⁻⁵.

Tooth anatomy, as shown in Figure 2.1, is made up of inner components and an outer layer of dental enamel. Dental enamel is the hardest part of the tooth and protects the inner regions from external attack. Nonetheless, it is prone to acid attack and wearing of dental enamel is possible as shown by controlled laboratory experiments in the literature. Control of dietary habits and constant salivary exchange prevents the degradation of tooth structure, since saliva has been known to protect the surface by forming a pellicle layer⁶. The selective permeability of the salivary pellicle layer has been discussed with respect to acidic buffers. The pH of the local oral environment dictates the breakdown occurring on the surface of dental enamel.

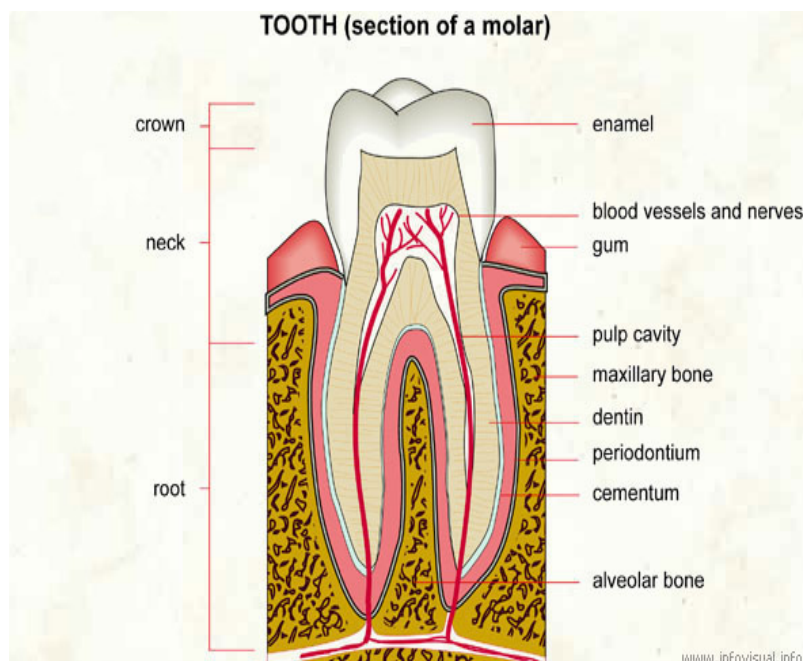


Figure 2.1: Dental anatomy

To prevent cavitations due to pH, maintenance of a healthy tooth structure along with good dietary habits is essential. However, understanding the structure of dental tissue has been a challenge for many in the scientific community. The caries disease has significantly disappeared since the turn of the 20th century, because of increase of fluoride in drinking water, though caries is still a serious problem. Fluoride is known to contribute in a significant way to the restoration of dental structure, but complete alleviation of caries is still a challenge and a goal for today's researchers.

This investigation aims to study dental enamel demineralization with Raman to characterize changes in chemical composition. Lesion progression that occurs over a period of days, *in vitro* is likely due to changes in carbonate solubilities in apatite, phosphate loss and hydroxyl (OH) or organic molecule substitutions. These bring about characteristic changes in the dental enamel structure that promote the growth of carious

lesions. To explain this further, we must have background knowledge of the role played by various other factors such as saliva, bacteria and acids that are present in the oral environment periodically. However, such a detailed analysis would make characterization of dental lesion formation very complex. Hence, ignoring the effects of saliva and bacteria, this thesis aims to study changes in the tooth microstructure, specifically surface areas of human dental enamel. Tooth structure is highly variable between primary and permanent teeth and has been discussed in the literature^{7,8}. Age, sex and disease are contributing factors and they can possibly influence lesion formation due to dynamic changes occurring in the salivary pH and bacterial accumulation on the dental surface⁹. Due to these variable factors, dental lesions have been hard to characterize¹⁰.

The structure of dental enamel lesions is quite complex and the presence or absence of certain features on the dental surface can influence the way the lesion is formed and progresses¹¹. Lines, grooves and other dental faults could possibly dictate the movement of ions within the structure¹². These ions are involved in a coupled diffusion process that leads to the development of a complicated lesion structure (sometimes they are called “white-spot” lesions). Recently, various mathematical models have been described in the literature to account for these changes¹³⁻¹⁶. This “white-spot” lesion formation can be explained simply from a technical perspective, but it is often characterized by changes occurring over months or years and is capable of being arrested as a result of changes in the lesion structure¹⁷. This arrest of the lesion is potentially quite significant as it protects the tooth’s interior and may help prevent the formation of a cavity¹⁸. Dental Structure is very anisotropic, with prisms to contain several orientations of the crystal structure^{16, 19},

²⁰. This has been affected during crystal formation, nucleation and growth as shown in figure 2.1 and figure 2.2 below. Due to the complexities of the enamel structure a good basis for a mathematical model of lesion formation could be obtained using an isotropic structure that would give an approximate understanding of how dental lesions form by demineralization and remineralization^{2, 21}.

Dental structure although anisotropic, is subject to breakdown in a surprisingly isotropic manner when exposed to acid attack *in vitro*. This is clearly reflected in the Raman spectrum obtained using polarized Raman spectroscopy, as shown by Ko et al.²², where the peak intensities of the sound enamel varies depending on the polarization direction of laser excitation. This however did not hold true for carious enamel, suggesting that sound enamel is optically anisotropic while carious lesions are made optically isotropic due to demineralization.

One potential project aim might be to create a structure that is reasonably optically isotropic upon demineralization. This would help in generating a mathematical model, which is isotropic both in structure and function.

2.1.1 Dental enamel

Dental enamel forms the outermost covering of the tooth, protecting the inner regions from breaking down due to external mechanical damage and exposure to acidic or alkaline environment. The portion of the tooth below the enamel is comprised of an organic/apatite matrix called dentin, which supports the tooth's surface during repeated

loading and unloading, which occurs during grinding and mastication. Dental enamel along with dentine forms a composite structure that can withstand high loads. Humans have different kinds of teeth and they occupy various positions forming a dental arch.

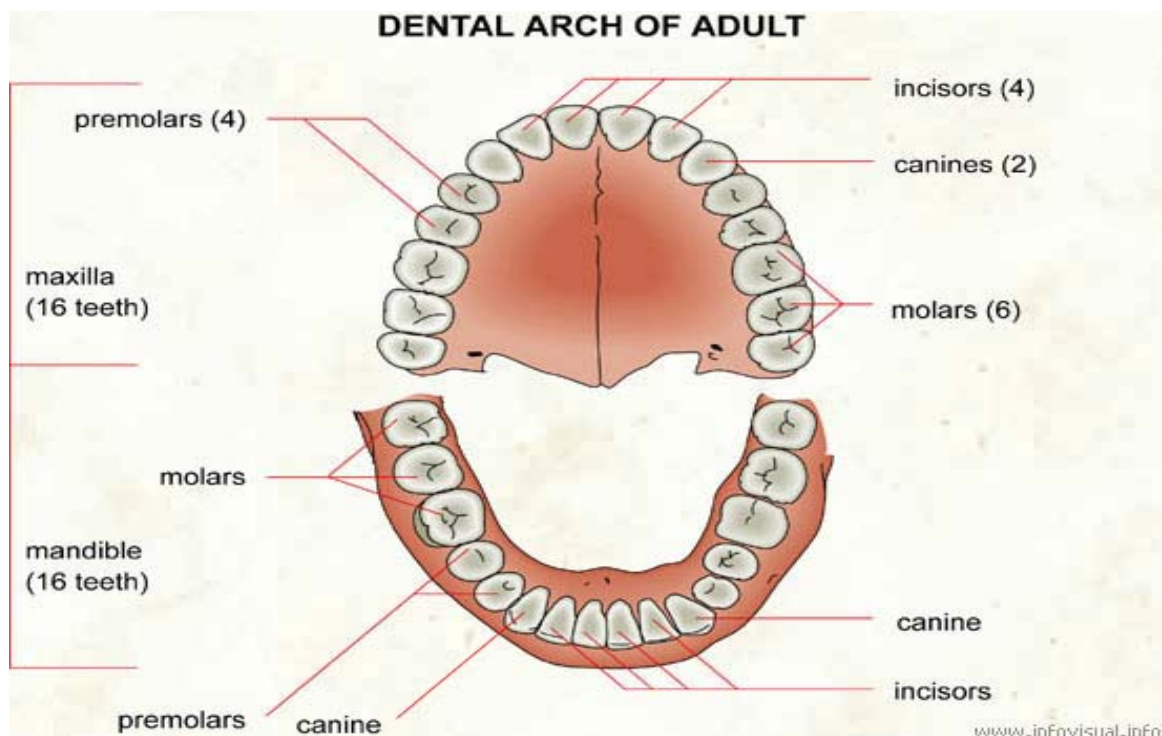


Figure 2.2: Dental arch

Initially, primary teeth occupy these positions in children and later, permanent teeth emerge from the same positions. These tooth structures vary in shape and size as they perform different functions in easing the mixture of food with saliva and forming morsels. Dental enamel, being the outermost layer greatly interacts with the oral environment and protects the inner regions of the tooth structure, that are the dentine and the dental root structures from chemical and mechanical attacks. The root structure promotes the exchange of nutrients from the blood into the dentine, which is responsible for the major biochemical changes occurring throughout the lifetime of a tooth and its underlying components. After eruption of dental enamel into the oral cavity, it is subject

to a variety of environmental factors, which can degrade the underlying dental anatomy. Dental enamel forms a barrier, protecting the inner components of a tooth from these environmental factors and pH changes. Since the dental enamel is at its most mature state at this point, it cannot regenerate or form further prism structures. However, remineralization of the tooth structure is possible due to various factors and lesions have been found in this arrested over a period of many years. This may be due to any of the salivary and dietary factors that increase the amount of bicarbonates, phosphates and calcium in the oral environment²³.

2.1.2 Microstructure of Enamel

Enamel is composed of crystals of carbonated calcium hydroxyapatite $[\text{Ca}_{10}(\text{PO}_4)_6(\text{OH})_2]$. Here, the hydroxyapatite lattice is impure, with carbonate substituting for phosphate²⁴. Carbonate is only present upto 3 –4 wt% in enamel²⁵, but is supposed to be responsible for crystallographic changes in the enamel structure making it susceptible to acid attack. Overall charge balance is essential along with a geometric fit within the crystal lattice to keep the structure resistant to ionic exchanges²⁵. The remaining 10 to 20 % of organic matrix and fluid constituents pack the structure together with hydroxyl (OH) bonds dominating the structure²⁶. Whether these are homogenous and or aiding demineralization of the chemical bond structure is still under investigation. Raman spectroscopy is potentially a powerful tool to investigate these carious lesions. Whether it would aid in understanding the lesion's structure and remineralization is the subject of this investigation²⁷.

A number of different inhomogeneous structural features have been found in sound enamel including tufts, spindles, pores and prismatic columnar structures. Transmission electron microscope (TEM) studies depict these near the dentin-enamel junction (DEJ), particularly exhibiting areas of hypomineralization²⁸. Bundles of crystals come together to form long prismatic structures that extend from the dentin to the enamel surface, oriented in a fashion to protect the inner layers of the tooth's structure from damage²⁹. Shown below is a picture from Breschi et al., performed via FEISEM (Field emission in-lens scanning electron microscopy) which shows prism layers oriented in both longitudinal and parallel direction. Magnification of that image is shown next to it.

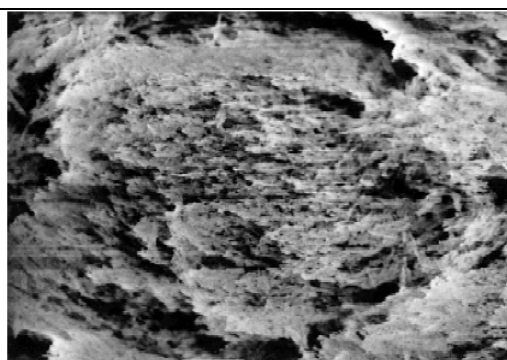


Figure 2.3: FEISEM image of dental enamel magnified to x14000 (Adapted from Breschi et al., 1999)

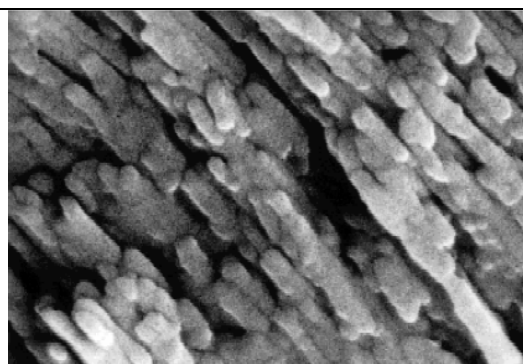


Figure 2.4: FEISEM image of dental enamel magnified to x20000 (Adapted from Breschi et al., 1999)

The earliest attack of the core enamel structure takes place at the striae of Retzius. These are found at certain prism boundaries and are formed naturally during tooth maturation. Extending deep into the enamel structure, they can help in the formation of caries, resulting ultimately in cavities³⁰. Furthermore, attack occurs through the cross striations of the prisms, and finally into the prism core. These structural features appear during the process of enamel formation and are known to allow for demineralization, during acidic

attack. They allow for acid from bacteria in plaque and other dietary factors to seep in through interstitial spaces and attack the core enamel structure.

2.1.3 Lesion Microstructure, pore and lesion zones

Lesion structure is characterized of four zones primarily, and each is identified by means of molecular methods or physical methods that examine optical properties such as birefringence. Enamel is typically translucent and lies over the dentin and has a considerable thickness, which depends on its location and the type of tooth. In a lesion the advancing front is the translucent zone, and can easily be segregated. Inside the translucent zone, there is an opaque structure called the dark zone. The majority of the lesion is also translucent. The surface of the lesion is white and opaque in lesions produced by more than three days of acid exposure. When the lesions are advanced, they can be observed without drying and look like white spots, typically being called “white-spot” lesions. The refractive index of enamel is different when exposed to air or water. When wet the refractive index is the same as water and hence no “white-spot” is observed. The difference in refractive indices between enamel and air can be observed by air drying, since the surface is rendered opaque. *In vitro* lesions are considered advanced beyond a period of about 5 days.

Translucent zone:

This is the advancing front of the lesion, but it is not always present. Loss of mineral from the prism structure is not detectable at such an early stage with microradiography or intrinsic birefringence³⁰. Porosity of the translucent zone varies between 1-2%, the same

as the surface zone. It is believed that mineral loss is low in the translucent zones, because no phase changes are observed. Since this optical measurement is highly variable across lesion zones, it was not considered for mapping measurements in this thesis. Degradation in this literature study was quite low to allow for a “white-spot” lesion to be observed. Furthermore, arrested lesion formation and/or remineralization are unlikely based on the facts available in the literature for this lesion zone.

Positively birefringent (dark) zone:

This region is very close to the advancing front of the lesion or the translucent zone. This region has been segregated by exposure to imbibition media, such as water or quinilone. Its porosity has been determined to be around 2 – 5 %³⁰. It contains minerals of hydroxyapatite and can remineralize on exposure to remineralizing agents such as fluorine, calcium and phosphates found in saliva. Salivary presence of fluorine is due to its presence in drinking water. Fluorine has been shown to be inherently present in the tooth structure and exposure to remineralizing agents can drive up the concentration of molecules from the oral cavity into the lesion structure to form a stronger apatitic phase. During this process the surface zone acts as a protective layer controlling the movement of ions through the structure. At this stage the caries process could be arrested or reversed depending on various factors involved in the process. Transfer of ions occurring from the surface zone into the dark zone needs to be studied and, hence, only the body of the lesion and surface zone was mapped in this literature report to understand the lesions characteristic properties. The dark zone could not be easily segregated or analyzed and is thus not part of this thesis study, and hence was ignored.

Body of the lesion:

This is the largest zone of the developing lesion and is marked by its translucent appearance. It offers a pathway to the dark zone in the absence of a surface zone in advanced lesions. It is highly porous and its porosity has known to vary between 10 - 25 % depending on its depth in the lesion body. Since its porosity is higher as you go deeper into the lesion's interior, the deeper parts of the lesion body were ignored, as they were not easily characterized.

Surface zone:

This is the outermost surface of the lesion body with a porosity of 1-2%.

Further degradation occurs through ionic exchanges, which can result from changes in pH, temperature and the action of microorganisms. Experiments detailed by Moreno and Zahradnik., 1974 have revealed that a quasi-equilibrium state develops in the surface zone, with precipitation of the remaining matter to allow for equilibrium with the liquid phase, such that $\text{CaHPO}_4 \cdot 2\text{H}_2\text{O}$ (DCPD), hydroxyapatite (HA) and fluoroapatite (FA) would be observed in the enamel surface. Such diffusion gradients would act as a pumping mechanism to pump substances from the inner enamel space into the oral cavity. These pumping rates are defined as diffusion fluxes³¹. The cross-sectional area of the demineralization eventually decreases, as the lesion boundaries are cone shaped at the lesion progression front, causing collapse of the surface zone due to a reduction in the rate of precipitation. Plaque and saliva play important roles in controlling the transfer of

substances in and out of the lesion boundaries, eventually causing cavity formation in the oral environment. The viscosity of the buffer medium was varied by addition of calcium and phosphorous at a temperature of 25 °C to simulate saliva in the oral environment. From their experiments it was observed that the pH was the determining factor for formation of a subsurface lesion for a constant concentration of buffer solution and vice versa. Addition of calcium or phosphorous reduced the chances of cavitation at 75% saturation of buffer solution. Overall, their experiments reflected their ideas that the system is a quaternary system of diffusion fluxes, which is essentially called “coupled diffusion”. Calcium and Phosphorous in the saliva could aid in remineralization of the diffusion front provided that the lesion hasn’t surpassed the limits of cavitation. Saliva forms a pellicle layer, which is selective to certain ion exchanges and further work in this direction would aid in understanding the true nature of these diffusion fluxes.

2.1.4 Hydration Layer

Present between the lesion body and the outward salivary exchanges is a body of ionic exchanges to incorporate movement of ions into and out of the apatitic layer giving rise to a body of hydration layer capable of promoting growth of apatite³². This hydration layer is analogous to a biofilm or a salivary pellicle in this thesis.

| Apatite lattice | Structured hydrated layer | Solution |
|-----------------|---------------------------|---------------------------|
| | HPO_4^{2-} | Ca^{2+} |
| | Ca^{2+} | HCO_3^- |
| | CO_3^{2-} | Pr HPO_4^{2-} |
| | | Ca^{2+} |
| | | H_2PO_4^- |

Figure 2.5 Hydration layer (Adapted from Cazalbou et al., 2004)

2.1.5 Arrested Lesions:

Fluorine (F^-), Chlorine (Cl^-), or other negative ions that have strong affinity to the biological substrate can also occupy hydroxyl sites in biological apatites, which may alter the buildup of protein structure and remedy the breaking of bonds further arresting lesion development. Lesions have been known to be present in this arrested state for a number of years and they prevent the further degradation of proteinaceous material, thereby preventing further degradation to lesion structure. Tooth structure also contains many other anionic species in place of the hydroxyl (OH^-) ion. These could be either fluorine F^- or Chlorine Cl^- and can bond with calcium Ca as a monovalent ion. Calcium bonds to oxygens in the phosphate groups and to another of the monovalent ions forming a triad structure, which supports the local charge balance²⁵.

Most papers in the literature argue that either carbonate or proteinaceous material breaks down first leading to lesion development. This data has been observed in either hydroxyapatite discs synthesized with carbonate, solutions or powders. Synthesized hydroxyapatite (NIST OHAp standard) displays a Raman peak at $962.2 \pm 0.16 \text{ cm}^{-1}$ and

the base shift is observed in geologic apatites has been rendered to the carbonate content in these apatites²⁵. However, demineralization has been consistently observed in both synthetic as well as other apatites. The data obtained has been characterized by various means and does not adhere to standards. This thesis aims to accomplish means by which an isotropic analysis could be put forward to understand lesion formation. Previous micro-radiographic studies do not account for the qualitative changes occurring across the lesion structure and this makes understanding of remineralization complex without the means to establish these changes. The data obtained by Raman analysis has been shown to be highly accurate by past studies and this thesis aims to further this knowledge and ultimately apply it to a mathematical, isotropic model by characterizing changes to the lesion structure that occur during experiments. This thesis will also refer to the past work in the literature and its implications to tooth microstructure and to a full understanding of how this may affect human physiology.

CHAPTER 3

MATERIALS, METHODS AND CHARACTERIZATION TECHNIQUES

3.1 Selection of teeth for testing

Five human premolars, extracted from human cadaverous donors and checked to be free from any evidence of caries were obtained from Church & Dwight, Inc.. The teeth were cleaned thoroughly with toothpaste and water to ensure removal of any kind of debris and split into two groups; one tooth was used as a control and one group containing 5 teeth was used for the growth of caries lesions over the course of 5, 7, 9, 11 and 14 days. The teeth were stored in 5% sodium hypochlorite solution and placed in a refrigerator at 5 °C until needed. There is a possibility that sodium hypochlorite may affect the biochemical structure of the enamel surface though no evidence exists for this. To ensure any possible effects were the same in each tooth they were all removed at the same time prior to investigation.

3.2 Preparation of control group teeth

The tooth structure in the control group was used to analyze the sound enamel and the various changes associated with it before it was demineralized. These enabled comparisons associated with crystallinity, carbonate substitution, amide I and III, between sound and caries enamel. This tooth was cut to remove the root. A diamond-wafering blade (Buehler® 1.5 HC Series) and a low-speed saw (Leco® Corp., Vari/Cut™ VC-50, St. Joseph, Michigan USA) was used under constant water irrigation. The tooth was then mounted root side down in a low temperature cure epoxy (SPI-

CHEM™, Westchester PA, USA) and allowed to cure for 8 h. It was proportioned as 100 parts resin with 24 parts of hardener. Once fully set, it was further sectioned in half from the lingual to the buccal side along the midline to reveal the cross-section of the tooth. The tooth was then ready for Raman Spectroscopy characterization.

3.3 Preparation of teeth for growth of incipient carious lesions

As shown in the figure 3.1 below, teeth used for lesion growth were coated with nail polish except for a 4 mm by 4 mm square on the enamel's buccal surface to ensure that demineralization always occurred at the same specific location. A 1 L glass dish was lined with wax (Cavex Set Up Regular, The Netherlands) and placed on a hotplate until the wax softened. The coated teeth samples were placed in the soft wax, root side down making sure that the exposed square of enamel was not placed in the wax.

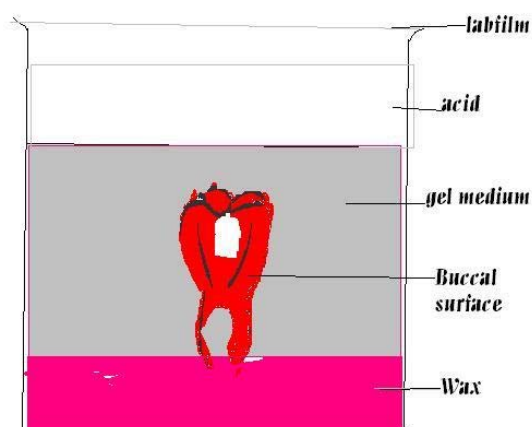


Figure 3.1: Picture depicting the procedure for the formation of dental lesions

Once the wax had solidified, 400 ml of 8% methylcellulose gel was poured on top and refrigerated for 4 h until solid. Filter paper was then placed on top of the gel and 200 mL

of 0.1 M lactic acid at pH 4.6 was poured over it. The dish was covered and incubated at 37 °C for up to 14 days. Single teeth were removed after periods of 5, 7, 9, 11 and 14 days and then rinsed in deionized water for 3 minutes to ensure removal of any residual demineralizing agents or mineral ions from the lesion surface. All samples were then subjected to removal of the root structure and embedded root side down in low temperature cure epoxy resin (SPI-CHEM™, Westchester PA, USA). These samples were then cut in half through the lesions from the lingual to the buccal side along the midline to reveal the cross-section of the lesion structure and tooth.

3.4 Formation of Bioglass

Bioglass was formulated with a composition of 52.2% wt. SiO₂, 23.8% wt. Na₂O, 4.2% wt. P₂O₅, 19.9% wt. CaO by melting in a crucible in a furnace at a temperature ranging from 1430 °C to room temperature. Precursor materials were sand (silicon dioxide – Riedel – de – Haen) 78.4 g, soda ash (sodium carbonate – Sigma Aldrich) 60.7 g, calcium carbonate (Sigma Aldrich) 44.5 g and calcium phosphate dibasic dihydrate (Riedel – de – Haen) 14.4 g. They were mixed thoroughly to ensure a homogenous composition of the final product. The raw materials used were analytical grade to avoid loss in bioactivity by trace elements, such as aluminum. First the furnace was heated to a temperature of 1300 °C and only half of the powder mixture was filled. This temperature was then raised to 1400 °C, to ensure the glass is melting adequately. The crucible temperature was lowered after 25 minutes of heating time and removed with tongs and appropriate fire protective gear. The remaining powder was added now, whilst gently mixing the slurry. This ensures that no bubbles are formed during the process, which can overflow and cause damage to the refractories of the furnace. A fused silica crucible (F-105 500 cc Ferro

Corp.) was used to avoid contaminating the sample. This sample was then brought back up into the furnace and the temperature raised to 1430 °C after 30 minutes.

An annealing furnace was heated to 600 °C and steel molds were placed on top of it to warm up the steel surface. This gives a non-stick surface and allows the glass to cool down gently. Then the glass mixture was removed from the furnace and poured over the steel surface in to the desired shapes. Before cooling, the glass was picked up with a steel spatula and placed in the annealing furnace. The annealing furnace was programmed as follows:

- 600 °C, Dwell, 10 mins
- 600 °C to 350 °C, 1 degree per minute
- 350 °C to 22 °C (Room temperature), 10 degrees per minute

At this point, the furnace was turned off and allowed to cool overnight until the glass samples have reached room temperature. The glass samples were then used to try growing lesion like structures in an isotropic bioceramic.

3.5 Characterization of Caries lesion through Raman spectroscopy

Micro-Raman was used to characterize dental lesions chemically during this investigation. The study of chemical composition of tissue structures is important in biomedical materials because of the sensitivity of biological systems to the local chemistry. In this investigation, we characterized dental lesions using Raman spectroscopy to help understand the distribution of various ions across the dental lesion structure. We only examined the main body and surface of the lesion to limit the amount

of data collected. Examining the whole lesion would complicate the process since the porosity of the lesion structure varies greatly between the dark and the translucent zones. Also, the dark and translucent zones are hard to segregate across the various lesion structures grown over a period of 5, 7, 9, 11 and 14 days.

Raman microspectroscopy uses an optical microscope to focus laser light which has a wavelength in the near IR or visible region on the sample. The laser light intensity has to be controlled in order to avoid sample damage due to heating effects. Raman relies on inelastically scattered photons. Laser light is either absorbed by the sample or reflected, some of it at a slightly different wavelength to the incident light. The energy of the light is proportional to its frequency. This scattered light is detected using a spectrophotometer and then displayed as a 'spectrum'. The difference between the incident light frequency and reflected light frequency shows up on the spectrum as an intensity peak. Peak ratios provide further information on the molecular composition of the sample in the case of Raman microspectroscopic methods. Most light is scattered in the form of Rayleigh light scattering, which is generally elastic. About one in ten millions of this light is scattered inelastically, which is then analyzed by a detector and software to give the molecular composition of the tissue sample³³. Advances in technology have permitted the use of highly sensitive detectors that make Raman effective in biomedical applications. Quantitative data obtained in this way is suitable for extracting statistical information from the Raman spectrum regarding chemistry and morphology.

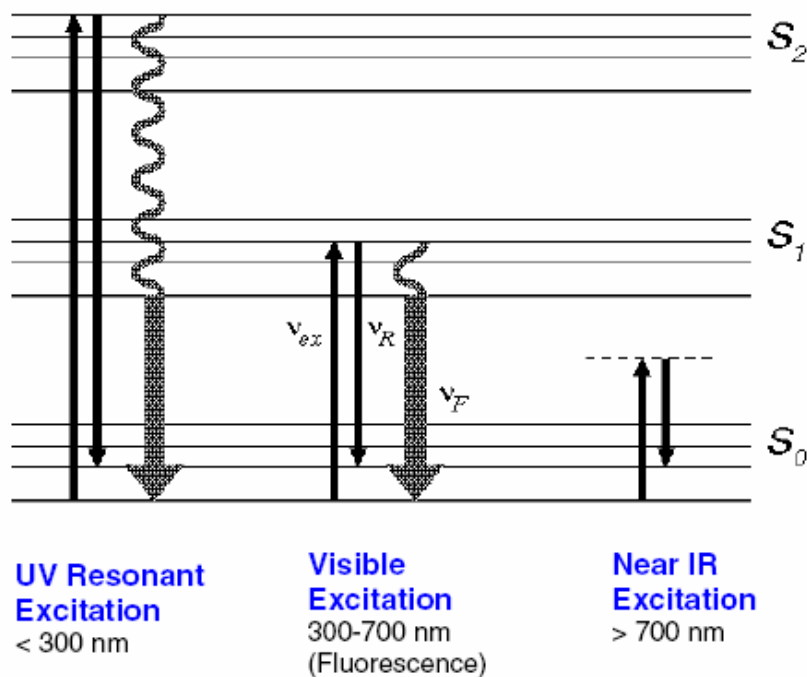


Figure 3.2 Raman effect: UV, visible and near-IR excitation strategies.

S_0 , ground electronic state; S_1 and S_2 , excited electronic states. The horizontal lines indicate vibrational energy levels. The diagram shows how a molecule in the ground state, S_0 , can make a transition from the lowest vibrational level to the first excited vibrational level by means of Raman scattering. Black uparrows indicate the frequency of the laser excitation light; black down-arrows indicate frequency of the Raman scattered light. The difference in length between black up- and down-arrows indicates molecular vibration frequency. Grey arrows indicate frequency of the fluorescence light. Notice that Raman scattering at different excitation wavelengths, UV, visible and near-IR, produces the same change in vibrational energy; therefore the excitation wavelength can be chosen to avoid spectral interference by fluorescence. For visible excitation, the fluorescence light frequency and Raman scattered light frequency are similar. As discussed in section 2.1, this leads to intense fluorescence background in visible excitation Raman spectra. Near-IR light has too low a frequency to excite fluorescence, while for UV excitation, the fluorescence light frequency is much lower than the Raman scattered light frequency. Hence, fluorescence background in the Raman spectrum can be reduced by using UV or near-IR excitation³³. (Reproduced from Hanlon et al., 2000)

As shown in the figure 3.2 above, Raman can be carried out in three different wavelengths. The wavelengths below 300 nm are defined as ultraviolet (UV), and wavelengths between 300 and 700 to be visible, and above 700 nm to be near infrared (IR). This provides Raman shifts in various band locations that give a signature for a molecule. Band locations are very specific for different molecular bonds in materials. Phosphate has four different bond excitations for the phosphorus-oxygen bonds, and

hence can provide four peaks in the Raman spectrum in the near-IR region. The width of these Raman peaks can provide information on the quality of the mineral as the narrowing of the peak indicates higher crystalline in the material.

A Renishaw inVia™ microscope was used for this study with a 785 nm wavelength laser and a grating of 1200 l/mm. The laser was focused on each point of interest with a Leica DMLM, 20X objective providing an approximately 2 microns spot size. A map of 3 lines spaced closed together (~ 50 microns) and a total of 40 acquisitions each were carried out resulting in 120 acquisitions for each lesion. The microscope was used to focus the Raman close to the middle of the lesion where it is considered to be at its most mature state. All spectral acquisitions were performed in the 300 to 4000 cm^{-1} range. Signal to noise ratio and fluorescence background were minimized by employing 10 seconds of exposure time, laser power of 70% (350 mW), which was kept consistent for all sample (5, 7, 9 and 11 day lesions). The Raman spectroscopy was calibrated using an internal reference sample of silicon to a static measurement of a single peak at 520 nm.

The Wire2® software of Renishaw® was used to remove sample background fluorescence using cubic spline interpolation base subtraction. The spectrum was smoothed and phosphate ν_1 at $\sim 959.9 \text{ cm}^{-1}$ (PO_4^{3-} , symmetric stretching band), amide I at $\sim 1606 \text{ cm}^{-1}$ (C=N stretching band), amide III at $\sim 1325 \text{ cm}^{-1}$, CH_2 wag at $\sim 1450 \text{ cm}^{-1}$ (C-H bending band) and carbonate at $\sim 1070 \text{ cm}^{-1}$ (symmetric stretching band) peaks were identified. These peaks were then Gaussian-Lorentzian curve-fitted to obtain quantitative

data on the peak intensities, area under the curve, and width (full-width at half maximum, FWHM) of each spectral band component. The FWHM of phosphate ν_1 at $\sim 959.9 \text{ cm}^{-1}$ was measured to obtain crystallinity of the mineral (phosphate). The curve fitted data was put into an Excel® spreadsheet in windows and the calculations discussed in the following text were performed. Data was further plotted using the ‘errorbar’ function in MATLAB® (The Mathworks, Inc.) Mineralization was calculated by taking ratios of intensities of amide I, amide III, CH_2 wag, and carbonate to phosphate peak intensity. In dental structures, two types of carbonate substitutions are observed. If CO_3^{2-} ion substitutes for OH^- , it is called a type A carbonate substitution and type B if CO_3^{2-} ion substitutes for PO_4^{3-} . Type A carbonate substitutions (at $\sim 1108 \text{ cm}^{-1}$) were observed in the 11-day and 14-day lesion only indicating a presence of hydroxyl (OH) substitution in teeth. Since the intensity observations were so small to incorporate in the trend data, no specific analysis was possible with Type A carbonate.

CHAPTER 4

RESULTS

4.1 Change in crystallinity across sound enamel:

Sound enamel varies in its crystallinity* as shown in the following figure 4.1. It is known to increase from the interior to the surface with its highest value at the surface. Authors Ko et al.²² have identified the breakdown of enamel rods as the reason behind changes in biochemistry between sound and carious enamel. They inferred this by characterization using both normal and transverse excitations. In normal excitation the tooth structure was kept intact and the incident light was normal to the lesion's surface, whereas in transverse excitation the tooth was sectioned transversely to expose the interior tooth and lesion structure. As no difference was found in the biochemical composition for the lesions in either transverse or normal excitation mode, even when the polarization of the light was changed the change was attributed to the breakdown of enamel rods. Sound enamel showed differences between normal and transverse excitation. Thus, sound enamel is taken to be optically anisotropic, but when carious lesions breakdown the structural components it becomes optically isotropic. These changes in optical properties did not affect the crystallinity measurements given later. FWHM (Full-width at half maximum) was found to be between $11.643 \pm 0.3 \text{ cm}^{-1}$, which is very close to previous studies²².

* Crystallinity of the apatite phase is measured as $1/\text{FWHM}$

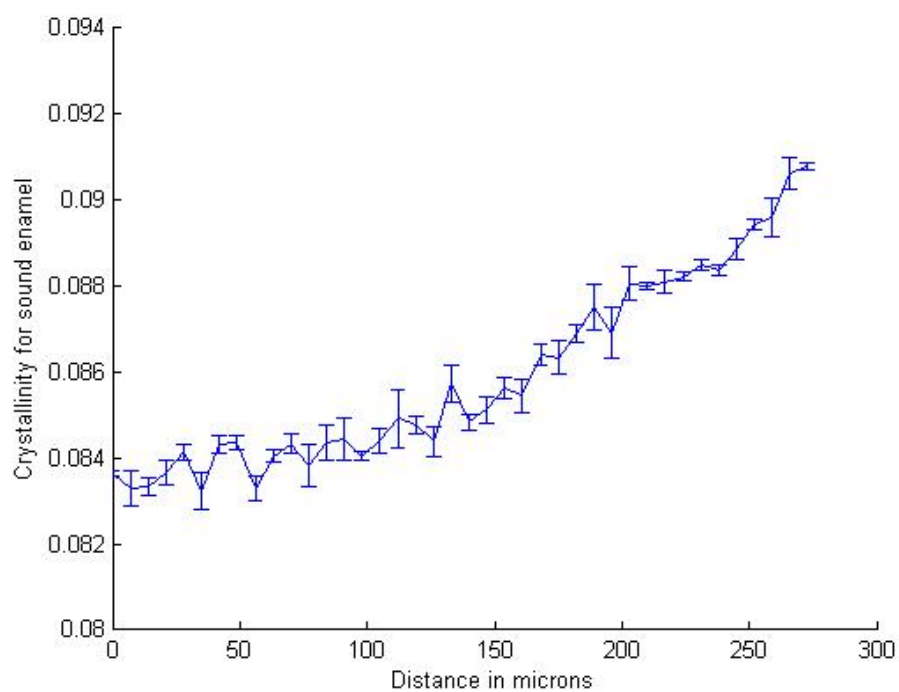


Figure 4.1: Crystallinity changes for sound enamel

The variations in crystallinity in most of the lesions did not differ significantly between sound enamel and carious enamel. Shown below are the crystallinity graphs with position for the 5, 7, 9, 11 and 14 day lesions. Note that the 14 day lesion did show lower crystallinity in its interior than the other samples.

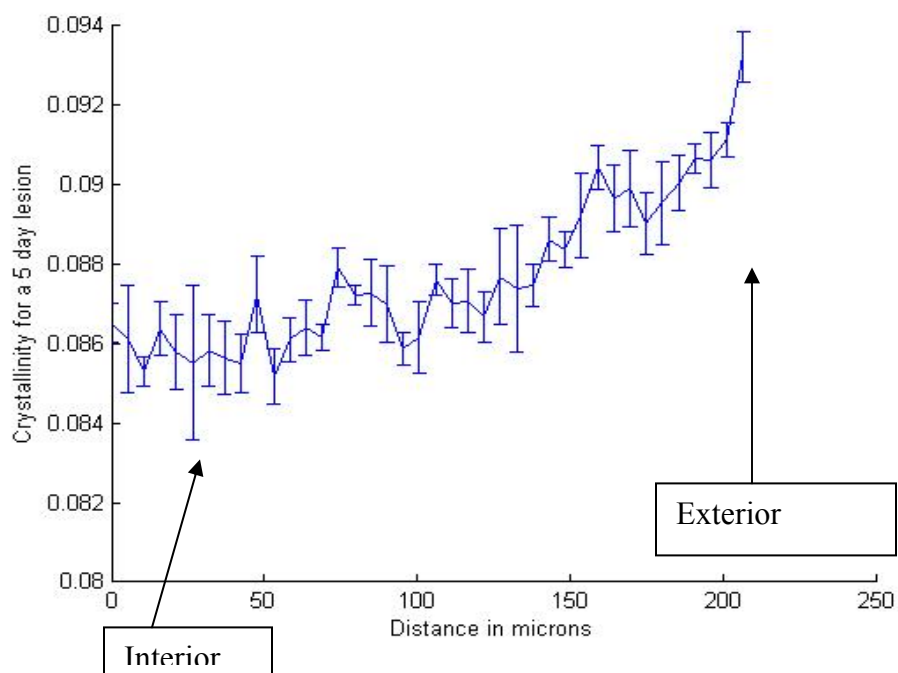


Figure 4.2: Crystallinity changes for 5 day lesion

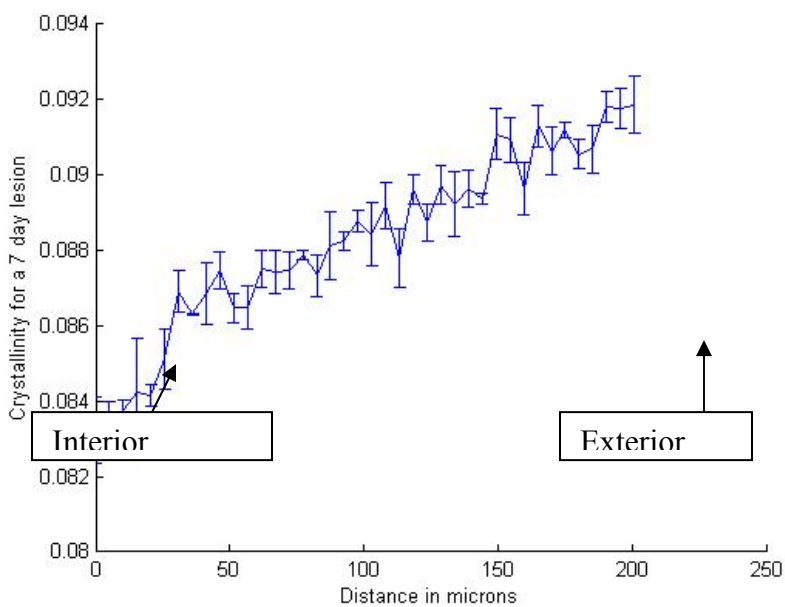


Figure 4.3: Crystallinity changes for a 7 day lesion

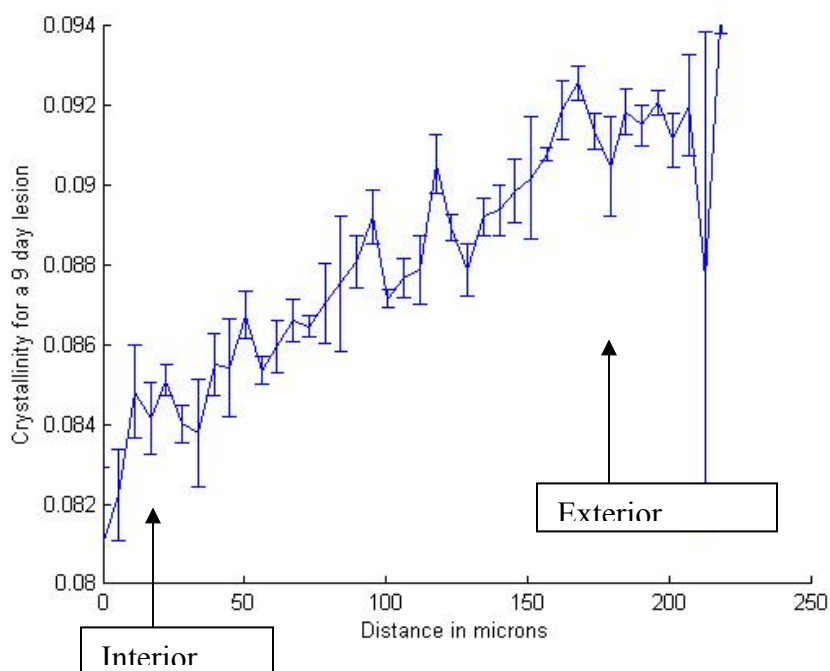


Figure 4.4: Crystallinity changes for a 9 day lesion

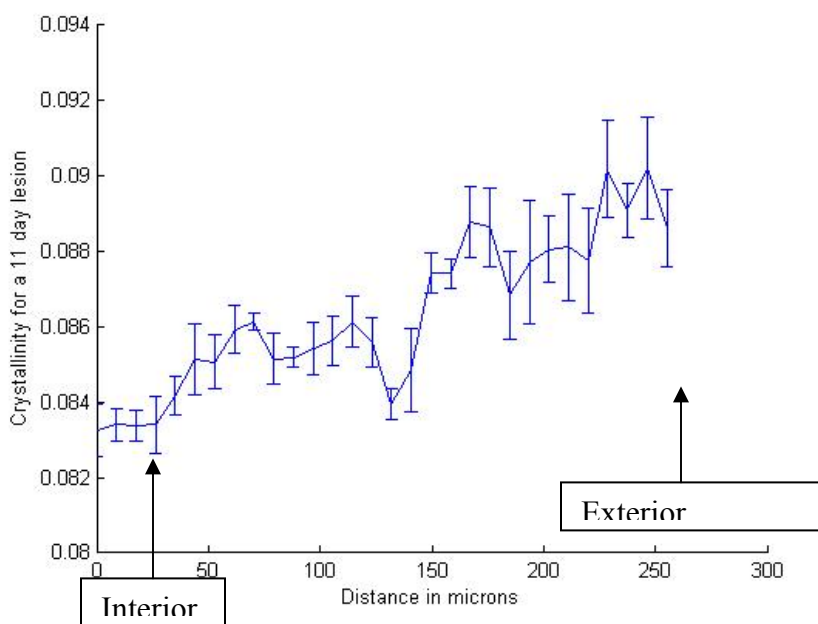


Figure 4.5: Crystallinity changes for a 11 day lesion

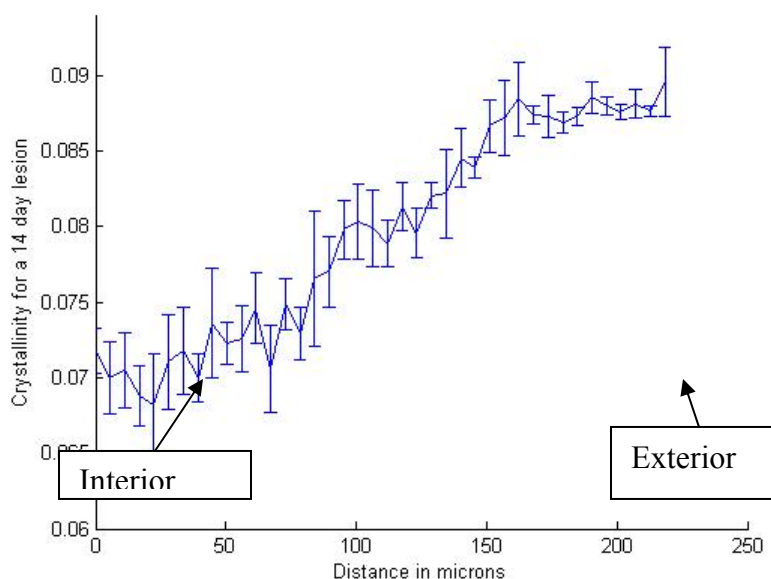


Figure 4.6: Crystallinity changes for a 14 day lesion

This data suggests that although breakdown of the mineral phase is occurring the crystalline phase that remains does not lose its crystallinity. Since acid has seeped through the crystallite, some of the fluid is held back in the lesion, rendering the lesion semi-solid. This is a form of “non-equilibrium crystallization”, which causes deviation from the actual composition and is more likely to occur in low-temp reactions such as this one³⁴. Thus, the change in crystallinity is not observed in lesions and this should be taken into account when studying lesion geometry. When the depth profile of lesions is studied the fact that there is an increase in the depths of the lesions with the period of growth must be asserted. These factors should be considered when building an isotropic model for lesion development *in vitro*. This will provide information regarding how lesions grow and the appropriate diffusion kinetics.

Comparison to previous studies:

It is believed that the surface zone forms as a result of ‘coupled diffusion’, and that the lesions develop subsurface^{35, 36}. Previous work illustrates this by means of chemical and nanomechanical methods of characterization the “white-spot” lesion. Presence of the lesion body has been shown, along with a surface zone, which stayed relatively intact and with the presence of different minerals (Fluorine, Chlorine, calcium, potassium, sodium). Diffusion occurs in two opposite directions, giving rise to a “coupled” process of simultaneous diffusing species producing a gradient leading to the formation of surface layer. Phosphate HPO_3 and calcium compounds, possibly $\text{Ca}(\text{OH})_2$ react in a ternary system of $\text{Ca}(\text{OH})_2\text{-H}_3\text{PO}_4\text{-Water}$ ³⁷ giving rise to dissolution products. This was done over a period of days 3, 5, 7 and 14 days, and showed reduced hardness and reduced elastic modulus of the carious lesions. As shown in the figure 4.7(b) and 4.7(f), calcium and phosphorous content reduces with a reduction in crystallinity in the interior of mature lesions. This is analogous to our study in which crystallinity variation as shown in figure 4.6 is lower in the interior of the lesion compared to 5, 7, 9 and 11 day lesions interior. This indicates that lesions are highly demineralized subsurface. In comparison, the surface is retained suggesting that lesions could be remineralized even after several days of acid exposure. Also it is interesting to note that the lesion in the surface zone is still of a high crystallinity (close to that of sound enamel), even after 14 days of acid exposure (figure 4.6 and figure 4.1).

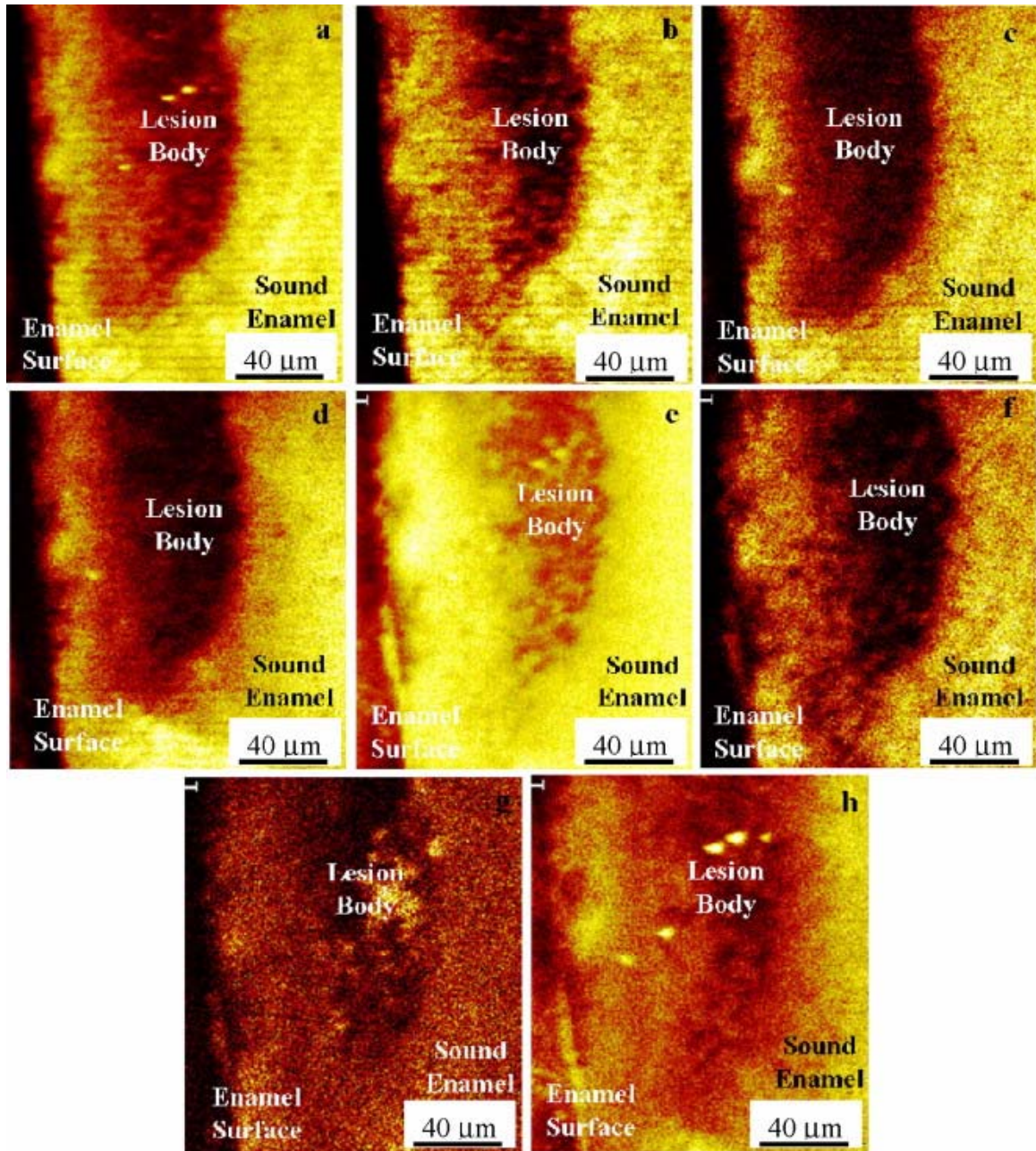


Figure 4.7: TOF-SIMS maps showing content of (a) total positive ion, (b) calcium, (c) potassium, (d) sodium, (e) total negative ion, (f) POxHy, (g) fluorine, and (h) chlorine through cross-section of lesion grown for 14 days in demineralization solution in human enamel (Adapted from Dickinson et al., 2007)

TOF-SIMS analysis, a chemical means of characterizing lesion structure, is somewhat independent of lesion porosity. In contrast, Raman is highly sensitive to changes in porosity and lesions that were porous could not be characterized in this study. Raman analysis takes into account lesion microstructural changes such as crystallinity, and

lesions have been characterized by considering the area under the Raman peaks. The area under the Raman curve is governed by its width, which corrects for changes in crystallinity. Several researchers have used this in the past to classify and analyze certain parameters contingent to their analysis.

Certain structural assumptions are a part of this thesis to understand the analogy between occupied sites in the crystal structure with the morphology of dental enamel. Dental enamel is not purely hydroxyapatite, but a mixture of other components embedded in a matrix of proteins and as such cannot be segregated without changing the basic structural morphologies^{38,39}. Understanding this analysis in a simple manner would require assumptions based on our knowledge of dental anatomy. This would help determine the transport processes and rates of chemical reactions in dental lesions along with previous knowledge of lesions behaving as a ‘molecular sieve’ to incorporate losses in the form of demineralization³⁰.

4.2 Change in carbonate across enamel:

Carbonate in the enamel structure is known to vary greatly, and can have pockets of relatively high concentrations⁴⁰. These can be explained by Raman investigation in this thesis. Shown below in figure 4.8 of carbonate variation in sound enamel performed by Raman Spectroscopy and Wire2® software in our laboratory. The data shows a close match to data in the literature, with little difference occurring between the interior of the lesion structure at 0 micrometers to the exterior of the lesion structure at ~250 micrometers.

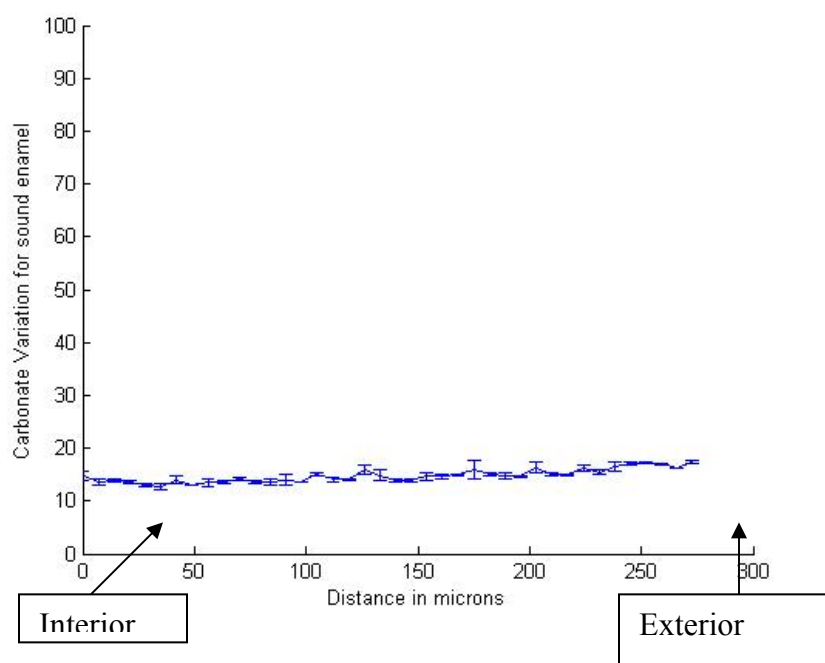


Figure 4.8: Carbonate Variation in Sound enamel

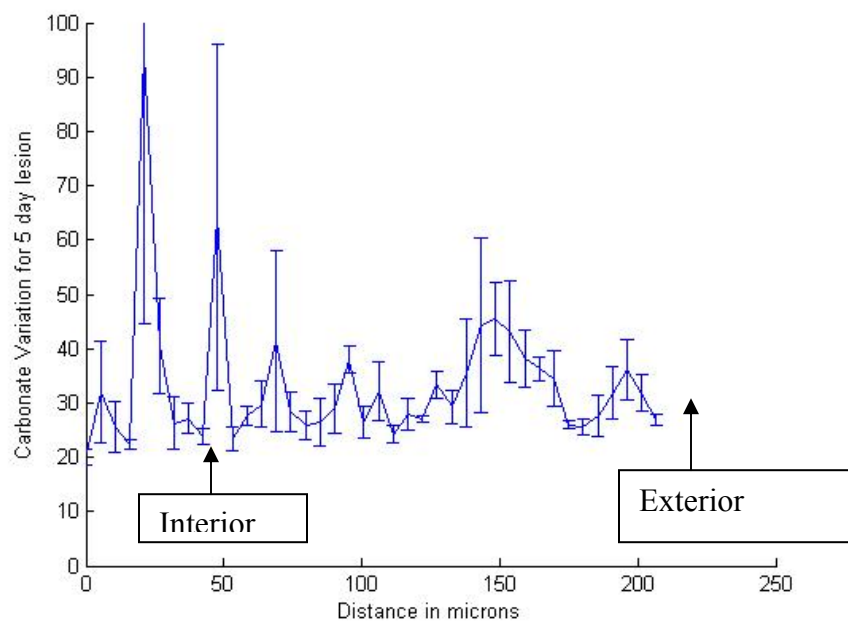


Figure 4.9: Carbonate variation for a 5 day lesion

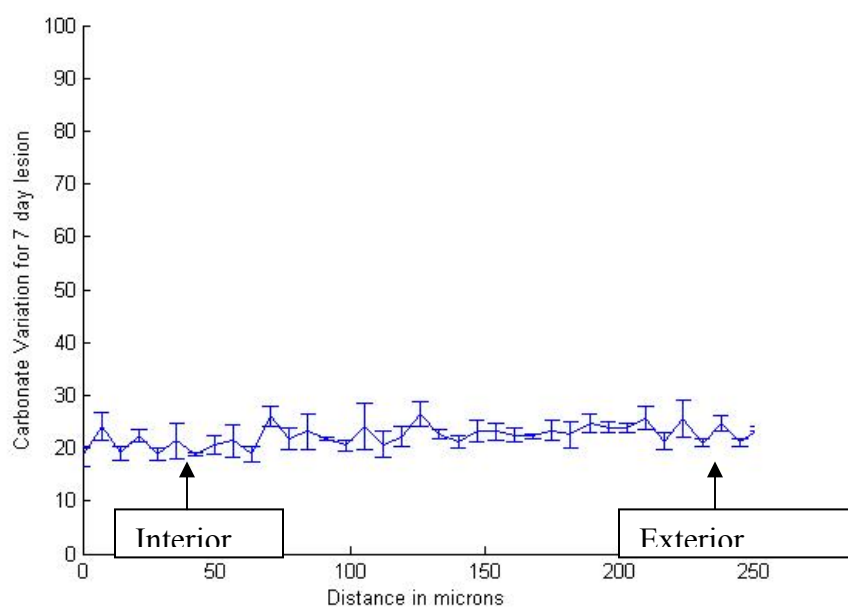


Figure 4.10: Carbonate variation for a 7 day lesion

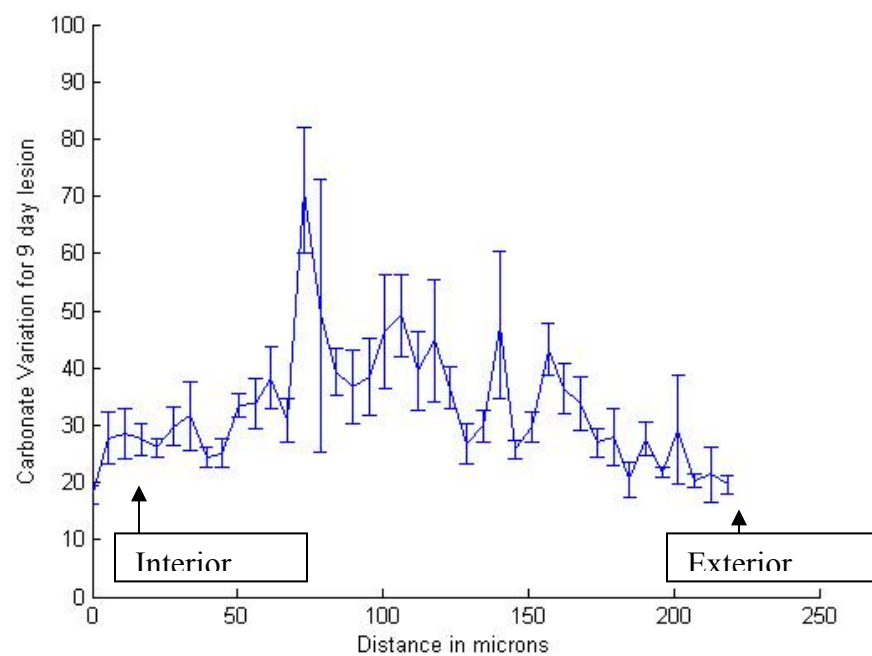


Figure 4.11: Carbonate variation for a 9 day lesion

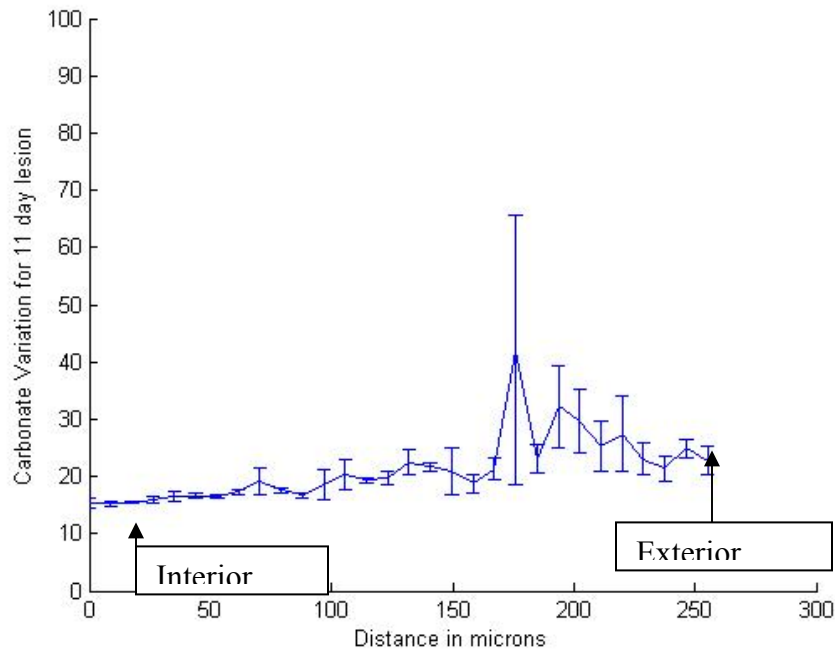


Figure 4.12: Carbonate variation for a 11 day lesion

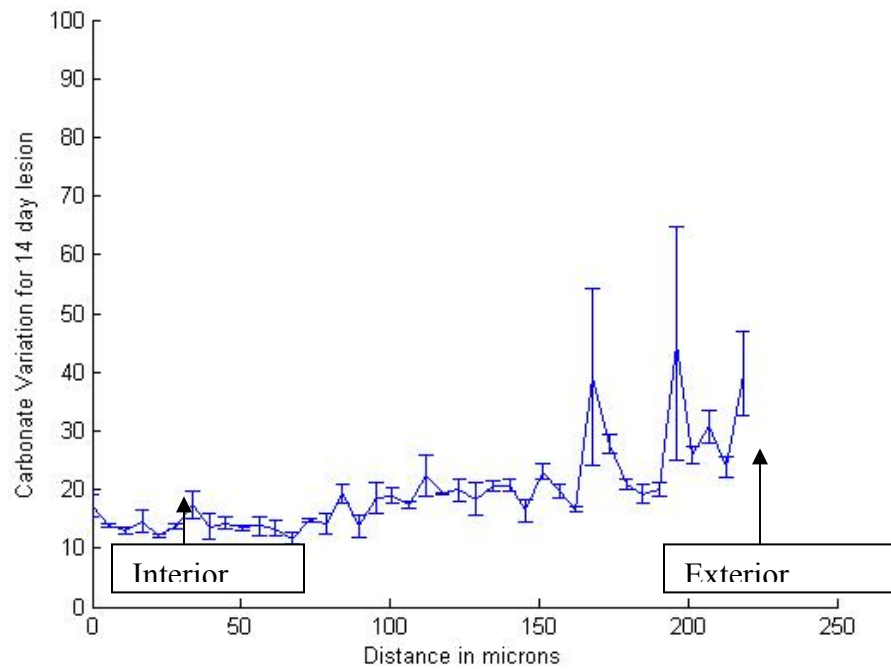


Figure 4.13: Carbonate variation for a 14 day lesion

The data shows a close match to data in the literature, with little difference occurring between the interior of the lesion structure at 0 microns to the exterior of the lesion

structure at ~250 microns. It is interesting to note that the carbonate to phosphate remains uniform across even mature lesions. This suggests the rates at which these ions are lost during demineralization are similar.

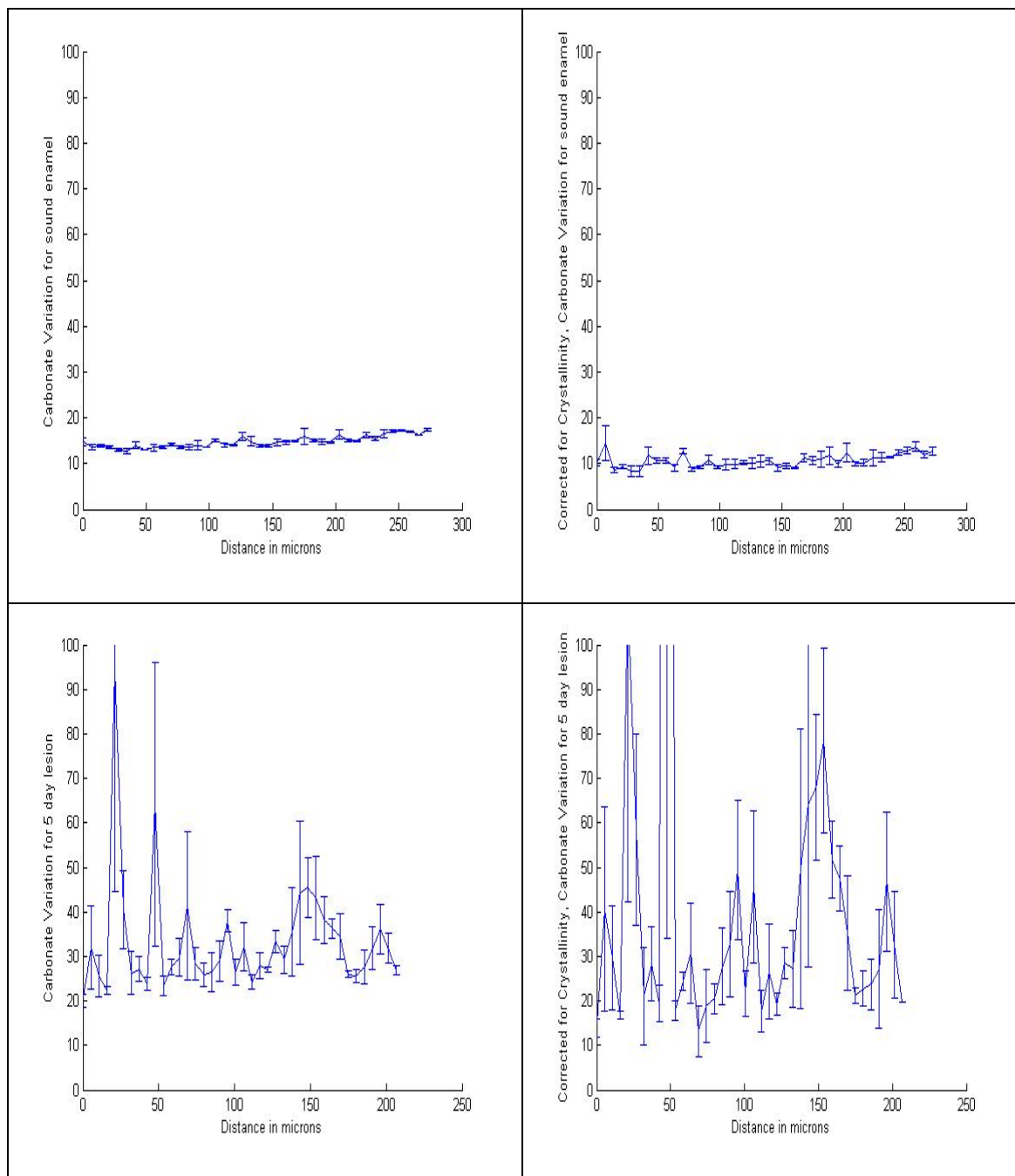
Previous studies of carbonate included XRD analysis, which involved pooled studies of synthetic carbonated apatites (CAP), and its crystallinity and other parameters, such as solubility. In a study by Baig et al., it was shown that microstrain, rather than crystallite size is the dominant factor in studying these parameters and dissolution phenomena⁴¹. In our investigation, we found that the crystallinity varies irrespective with the carbonate content. The carbonate content is found to be variable throughout even after dissolution for a period of days *in vitro*. Whereas, the crystallinity is steadily increasing from the lesion's interior to the lesion's exterior irrespective of the number of days of lesion formation.

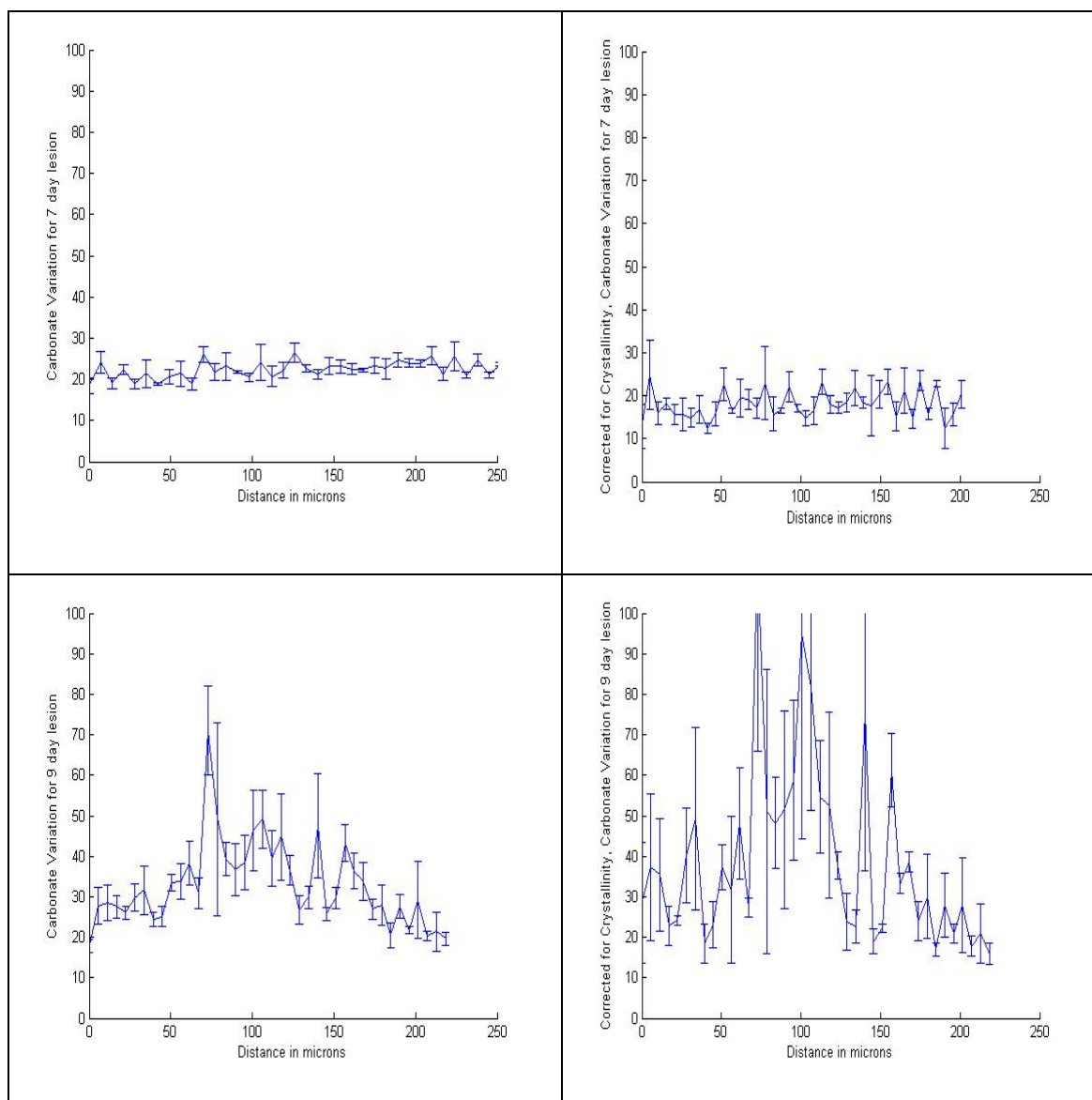
Raman accounts for the crystallinity* variation by considering area under the curve in our analysis. However, no change in the trend is observed between the raw data, and the one corrected for crystallinity in phosphate to carbonate ratio variation indicating that crystallinity is not a significant factor in determining the substitutions present or their dissolution. Although the crystallinity increases from the lesions interior to the lesion's exterior even in the most mature lesions, the same variation is not reflected in phosphate to carbonate variation, where area under the curve is taken into consideration (see table

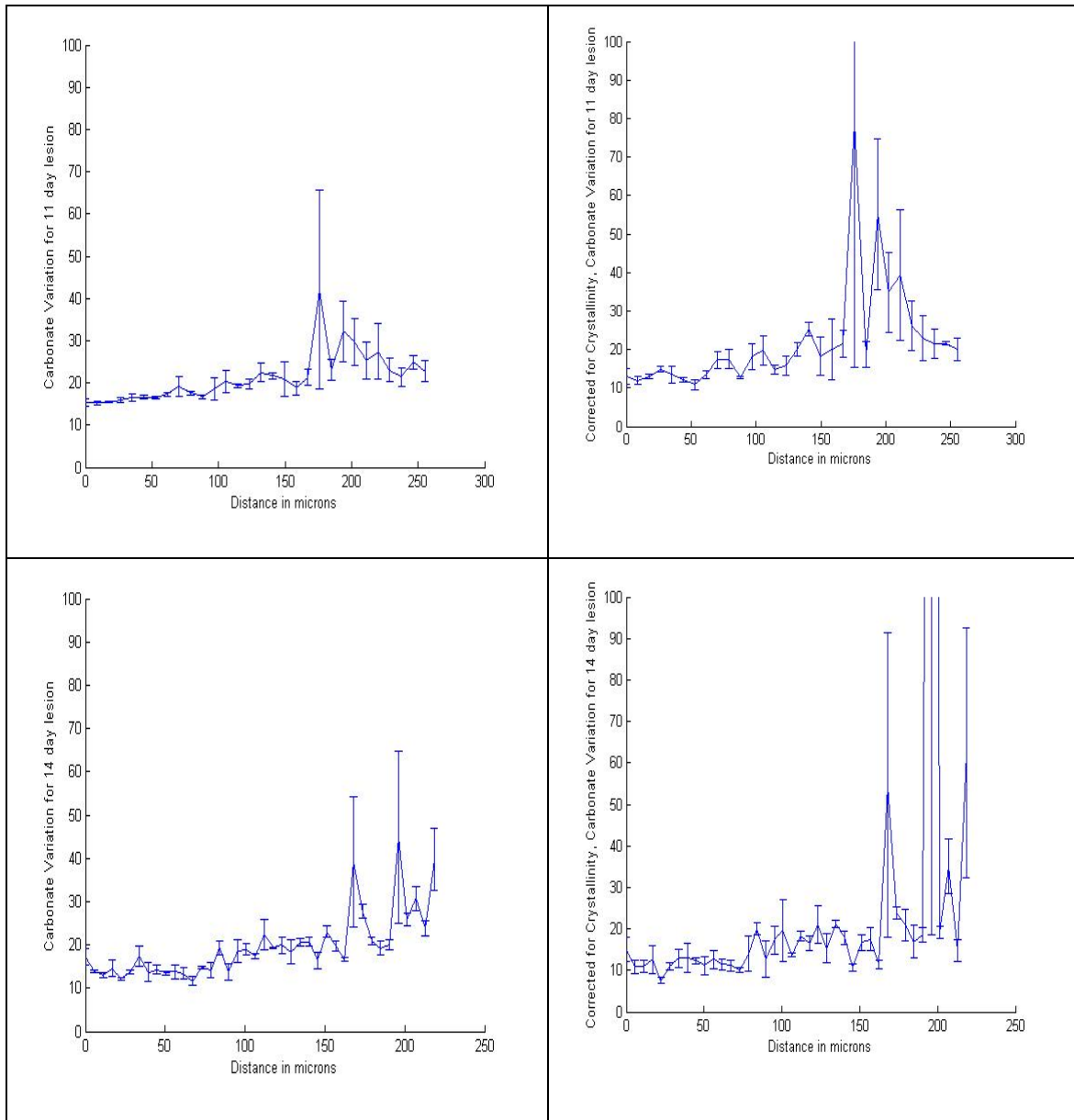
* Here the issue of crystallinity is dealt with in terms of the area under the curve, rather than FWHM as discussed earlier.

4.1). This reflects that the change in crystallinity of calcium and phosphate phases does not affect the variation of carbonate across lesion boundaries.

Table 4.1: Phosphate to Carbonate Variation for sound enamel and lesions of 5, 7, 9, 11 and 14 days







This draws attention to the fact that there is another factor, possibly ‘microstrain’ that affects lesion formation. Microstrain is defined as a form of lattice imperfection influencing the d-spacing within crystal domains⁴².

Enamel formation is a complex process, which involves the dentino-enamel junction (DEJ) responsible for the growth of crystallites into the tooth cavity. Ondoblasts and

ameloblasts extend into the tooth cavity increasing at different lengths depending on the deposition rate and forms structures such as cross-striations, striae of Retzius and perikymata grooves. Ameloblasts secrete these enamel proteins, which enhances crystal growth or retardation^{26, 43, 44}. Diurnal systems dominate the growth of enamel crystals and these are made more acid resistant during the growth process by calcium, phosphate and bicarbonate ions⁴⁵. Structural proteins include amelogenin (80 – 90 percent of total enamel protein), ameloblastin (5 – 10 %) and enamelin (1 – 5 %). Amelogenins are capable of buffering the enamel fluid by absorbing H^+ ions, which reduces the acidity of the surrounding matrix, thereby preventing dissolution during enamel formation. Enamelin is believed to be responsible for crystal elongation as it is restricted to the mineralization front between the rod and interrod enamel²⁶. Tooth structures that are more acid resistant have their carbonate contents degenerated during the enamel maturation process²⁶.

Understanding the formation of the enamel structure may lead to enamel being formed in the laboratory⁴⁶. This could then lead to a breakthrough in the area of dental restoration, and could be substituted for other techniques such as etching and bonding of false tooth structures.

4.3 Changes in protein structure across enamel:

Amide I has been ascribed to the peak at $\sim 1667\text{cm}^{-1}$, when scanned at 1064nm by investigators Kirchner and Edwards et al⁴⁷ using Raman spectroscopy. In our investigation a wavelength of 785nm was used to identify a peak at $\sim 1605\text{cm}^{-1}$

attributable to Amide I. This has not been reported previously in the literature. Shown below is the variation for Amide I across the lesion structure for 9 and 11 day lesions. This was observed only in lesions of 9 and 11 days. It is quite likely to be present in other lesions, but was not observed in any of the sound enamel mappings. To reiterate, this was segregated due to the effect that lesion degradation promoted it to be visualized in Raman spectroscopy. Thus, proteinaceous material present as Amide I is observed and characterized. As seen, it increases in one 9 day lesion and it decreases in the other 11 day lesion. Thus, we can safely assume that the distribution of amide proteins is either highly pronounced towards the surface of the lesion or it progressively decreases due to degradation of proteinaceous material during lesion development. This was not very clear in our observation due to time constraints and further work needs to be done in this direction. Further work could examine how changes in protein concentration may lead to carious development in certain areas of tooth structures or in certain individuals over others.

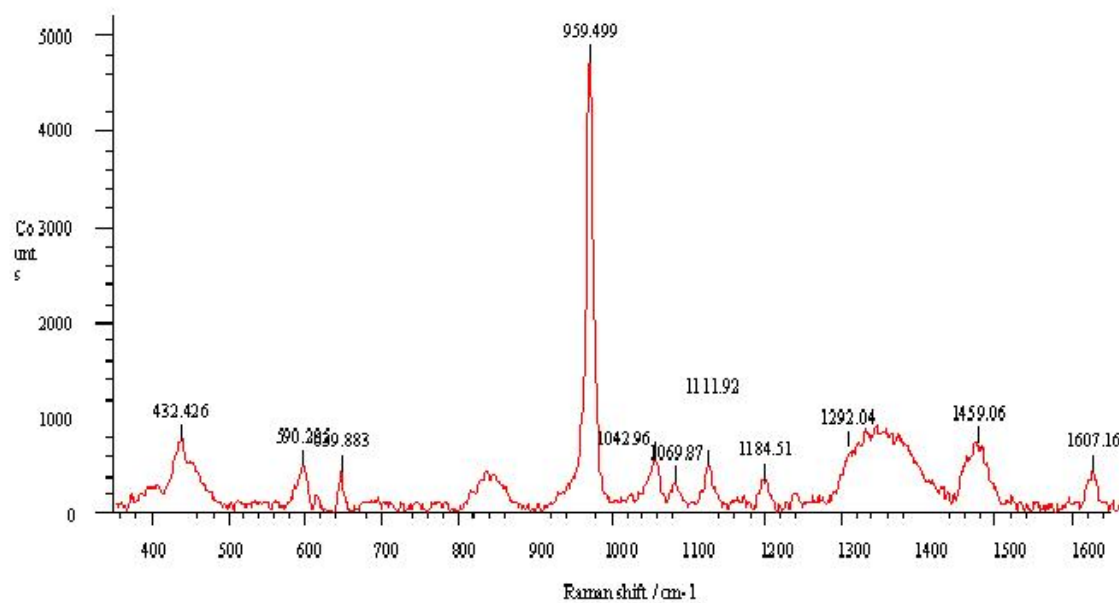


Figure 4.14: Raman spectrum of a dental lesion showing amide I peak at 1605 cm^{-1} , Amide III at 1305 cm^{-1} , carbonate type B at 1070 cm^{-1} , type A carbonate at 1111 cm^{-1} and CH_2 at 1450 cm^{-1} . Strong phosphate peak at 959 cm^{-1} is observed.

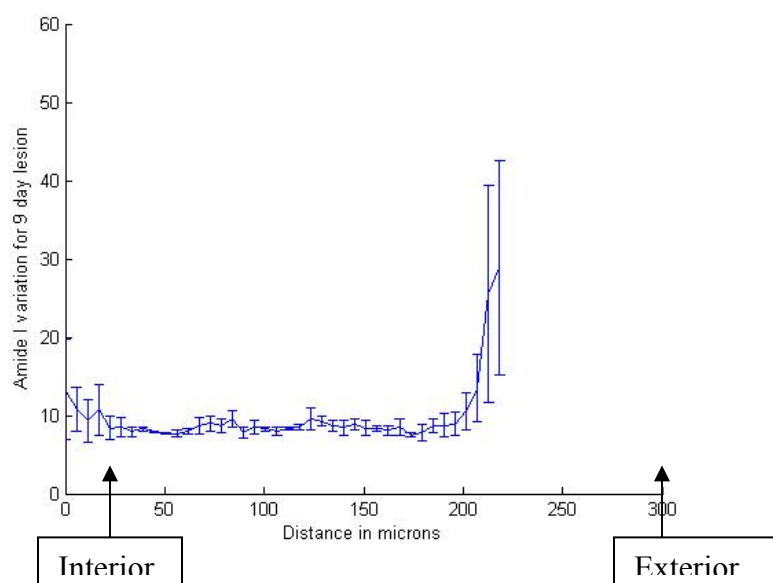


Figure 4.15: Phosphate to Amide I ratios for a 9 day lesion

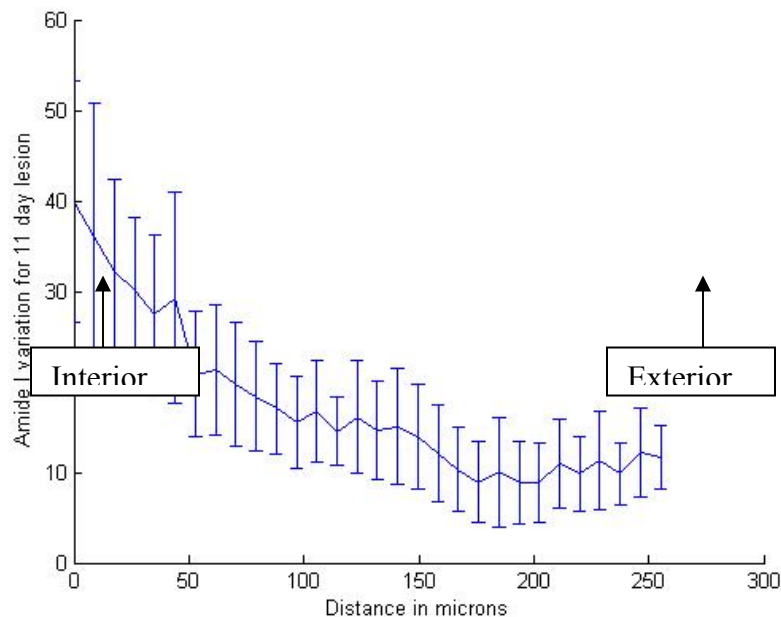
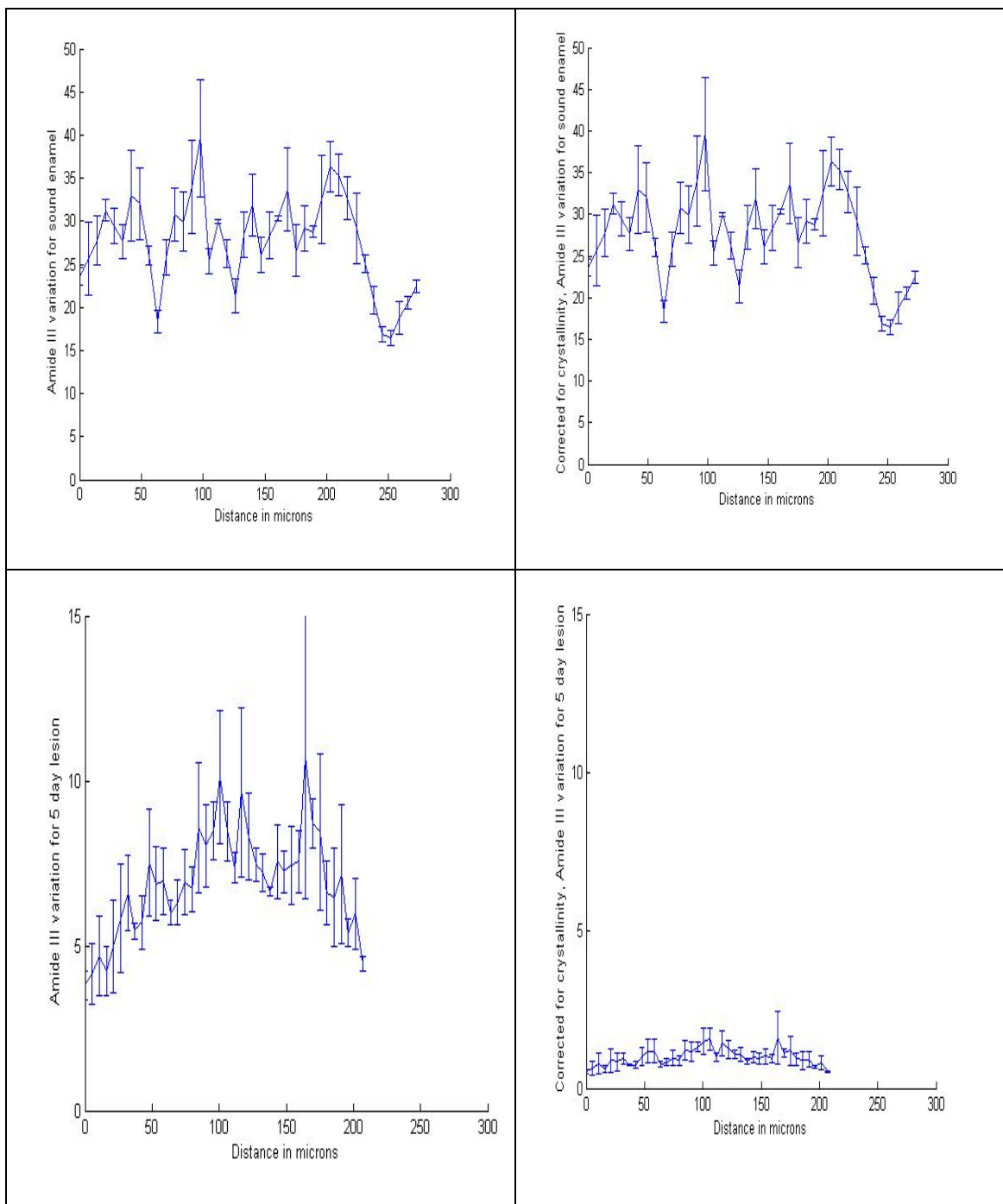


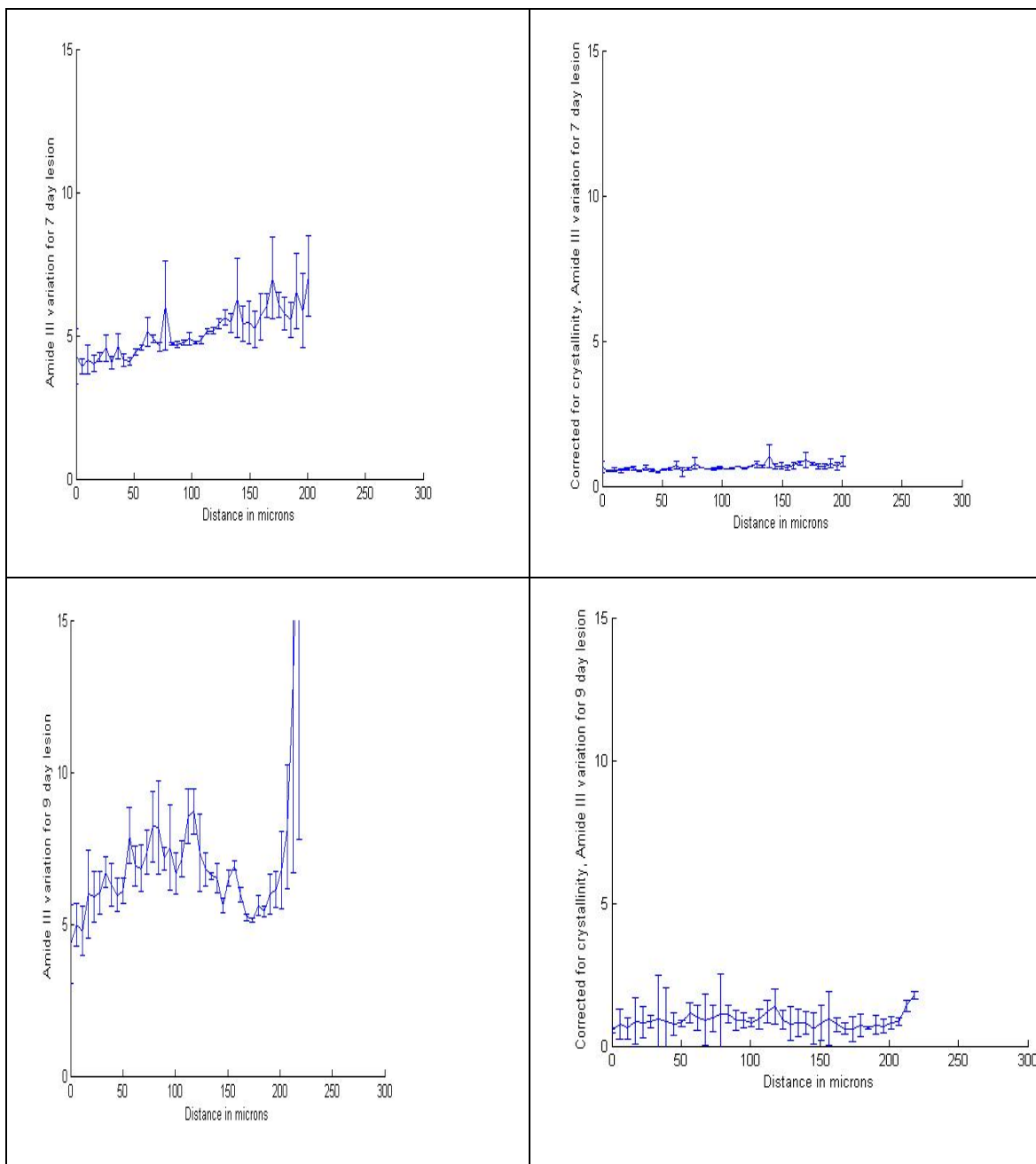
Figure 4.16: Phosphate to Amide I ratios for a 11 day lesion

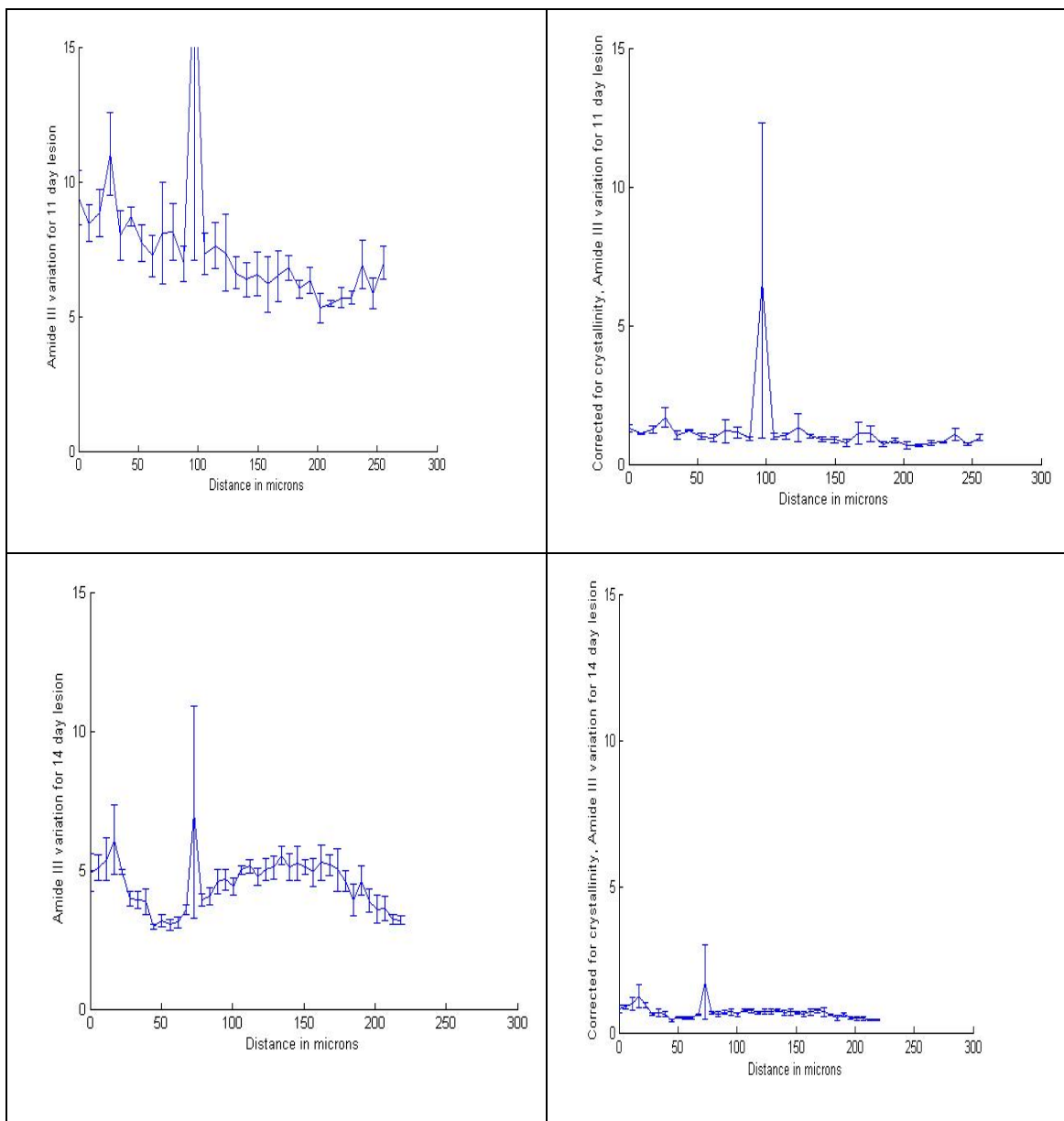
Shown below in table 4.2 is the data for Amide III obtained in our laboratory through Raman investigation. The value of the proteinaceous material after demineralization reduces but stays fairly constant throughout the lesion structure suggesting that the proteinaceous material does not degrade over time or extent of demineralization leading to the conclusion that during lesion development, the proteinaceous material is likely to be worn down chemically before being mechanically damaged. The mechanical damage can then result in further loss of hydroxyapatite structure. This fact has been hypothesized in the literature⁴⁸, where the authors state that the carious process begins by lesion development due to selective attack primarily along the prism boundaries when there is proteinaceous material present. This has been observed visually as the translucent zone in sound enamel. From here the loss occurs along the hydroxyapatite minerals, leading to the formation of a lesion structure³⁰. Since microRaman is a very sensitive technique, it is

likely that the results obtained may vary due to micro variations across the tooth structure.

Table 4.2: Phosphate to Amide III variation for sound enamel and 5, 7, 9, 11 and 14 day lesions







CHAPTER 5

DISCUSSION

It is known that Raman studies are very versatile and allow for easy characterization with little or no requirement for sample preparation⁴⁹. The combination of optical microscopy and technological advances has influenced Raman spectroscopy making it easier to characterize specimens with high resolution and good signal to noise (S/N) ratios as well as giving better qualitative analysis.

In this research the maturation of dental lesions has been studied over a period of 5, 7, 9, 11 and 14 days. It has been shown that the extent of demineralization during lesion formation increases with time. Also, variations in the crystallinity do not affect the degree of substitutional changes in the mineral during lesion formation. There could be another factor such as 'microstrain' that can modify the Raman peaks. This could possibly explain why the protein signal is stronger in the inner regions of the lesion, though this seems unlikely. The results regarding the carbonate substitutions and crystallinity changes match those reported in the literature on lesion formation. This indicates that Raman spectroscopy is potentially an effective method for the study of lesion growth, chemical composition and structure. Our study also demonstrated that certain organic peaks were visible after the 9th day. This indicates that the organic matrix remains intact during lesion formation even though the inorganic constituents have been broken down (notably the carbonate and phosphate). The use of Raman to study lesions could be further applied to measurements of tortuosity (a measure of how pore structure is

interconnected), density, transport processes and rates of chemical reactions. This will help in understanding the “coupled-diffusion” process occurring across the lesion. Also, it may be possible to use Raman investigations of the pellicle layer on the tooth surface during demineralization. In this case, demineralization must take place in the presence of saliva and the concentration of phosphate and carbonate at the surface can be measured to help understand the coupled diffusion process.

Our initial attempt with Bioglass® to study lesion formation in an isotropic media was inconclusive because of several experimental and time constraints. Bioglass was formed as shown in Chapter 3 – Materials, Methods and Characterization techniques. The lesions were grown in just the same manner as dental lesions. However, the changes observed in the Bioglass were minimal and hard to characterize because of lack of lesion depth and poor Raman peak measurements. Hydroxyapatite displays a phosphate peak at $\sim 962\text{ cm}^{-1}$. This is absent in the Raman data for Bioglass®. Thus, it would have been very hard to compare in terms of lesion formation and/or peak intensities. Another attempt was made to grow lesions in isotropic hydroxyapatite discs, but lesions were not observed at a pH of 4.6. Maybe, using a lower pH may aid in forming lesions in such materials. However, more work has to be performed experimentally to determine this and it was beyond the scope of this research thesis. Coupled diffusion in an isotropic material would be easier to model and could be of assistance in understanding carious lesion formation. This isotropic model could then be compared to the enamel histology and Raman analysis to determine differences in organic and inorganic chemistry.

CHAPTER 6

CONCLUSION AND FUTURE WORK

Carious lesions were formed and characterized using Raman Spectroscopy. Our study demonstrates that lesion formation over a period of days can be conclusively studied using Raman spectroscopy. The following important results have come out of this study:

- The crystallinity of the apatite varies with distance from enamel surface and a similar variation is seen in all lesions. A substantial drop in crystallinity is only seen in the most mature lesion. Even then it is only in the interior. This is in accord with previous results.
- The ratio of type B carbonate to phosphate substitutions in the apatite shows little variation across the lesions. However, structural inhomogenities and possibly experimental error gives occasional high values. These results suggest phosphate and carbonate ions behave similarly during demineralization.
- Type A carbonate substitution was also seen in the mature lesions. This may indicate that it is lost more slowly than type B carbonate substitution.
- Amide III was seen in all the Raman spectra. However, a Raman peak at $\sim 1605\text{cm}^{-1}$ was observed, which was identified as Amide I. This peak has not been observed before and has been characterized based on our understanding of existing literature studies involving Raman spectroscopy⁵⁰⁻⁵².
- The ratio of phosphate to Amide III appears to decrease with the maturity of the lesion. This suggests it may be a good measure of lesion development.

Further work would involve studying lesion remineralization, and its effects within the oral environment. This may include the study of the formation of hydroxyapatite and the

lesion structure as demonstrated in this thesis. The method of formation of hydroxyapatite can influence the way in which remineralization is observed *in vitro* within a gel formation^{53, 54}. However, much work needs to be done in this direction to understand remineralization and the phases formed since they may not even be hydroxyapatite. Also, such a study could involve major biochemical changes associated with dental enamel growth and biology and its correlation to dental research. Further work would require a greater understanding of the basic morphology of lesion growth including hydroxyl (OH) substitutions in terms of apparent solubilities, Type A carbonate substitution (Phosphate with hydroxyl) and the role it plays in dental lesion formation^{55, 56}.

As shown in our work, the study of enamel proteins was rather inconclusive. Further study could be performed on enamel proteins via other techniques and correlated with the present study to obtain information regarding the changes occurring during lesion formation and how this may affect its chemical or mechanical behavior. Similar studies could be used to relate the properties of sound enamel to the changes in its proteins with the use of genetically engineered mice to knockout selected proteins. Past studies using this method have been used to study the effects of aging and something similar could be used to study enamel proteins such as enamelin, amelogenin and ameloblastin⁵⁷.

CHAPTER 7

STATEMENT OF THE PROBLEM, SPECIFIC AIMS AND SIGNIFICANCE

7.1 Statement of the problem

Enamel surface, saliva and dietary components all form parts of the oral environment. If we were to get to the crux of the problem, saliva and diet are secondary factors. Hence, to say the least, teeth are important for mastication. However, tooth loss is quite likely in the cases of severe dental carious formation. Dental problems such as fillings, root canal and other restorative treatments are very inconvenient. Destruction of dental enamel can render the individual susceptible to toothaches and headaches. All of this begins at the dental enamel surface, making it the primary cause of most dental problems. Hence, studying dental enamel demineralization and remineralization would be the primary components of this investigation. This would be carried out specifically using Raman spectroscopy of dental lesions over a period of 5, 7, 9 and 11 day lesions. This will hope to accomplish the basic lesion structural changes over a period of days in terms of particle solubilities as it affects dental enamel dissolution. Enamel prism structure would be critical point that would guide this analysis along with carbonate substitutions, amide I and III substitutions and phosphate degradation.

7.2 Specific aims of this investigation

- 1- To validate mapping using Raman Spectroscopy as an alternative and as a site-specific method for studying the variation in enamel dissolution of a period of 5, 7, 9 and 11 days.
- 2- To develop an understanding of an isotropic model to study the kinematics involved in dental lesion formation, and thereby providing for a measure of reversing the process by remineralization of the “white-spot” lesion.

7.3 Significance of the problem

Dental lesion characterization in terms of carbonate solubilities would aid in understanding the mechanisms involved in lesion formation as it is believed that lesions form due to the presence of carbonate apatites links in hydroxyapatite.

REFERENCES

1. C. D. Gibbs; S. E. Atherton; E. Huntington; R. J. M. Lynch; R. M. Duckworth, *Archives of Oral Biology* **1995**, 40, (9), 879-881.
2. R. Z. LeGeros, *Journal of Clinical Dentistry* **1999**, 10, (2), 65-73.
3. L. Mandel, *Journal of the American Dental Association* **2005**, 136, (1), 71-75.
4. K. D. Jandt, *Trends in Food Science & Technology* **2006**, 17, (5), 263-271.
5. M. L. Hunter; N. X. West; J. A. Hughes; R. G. Newcombe; M. Addy, *Journal of Dentistry* **2000**, 28, (4), 265-270.
6. R. T. Zahradnik; E. C. Moreno; E. J. Burke, *Journal of dental research* **1976**, 55, (4), 664-670.
7. M. Takahashi; J. H. Zheng; K. Mori; I. Mataga; K. Kobayashi, *Materials Science & Engineering C-Biomimetic and Supramolecular Systems* **2006**, 26, (4), 703-706.
8. L. J. Wang; R. Tang; T. Bonstein; P. Bush; G. H. Nancollas, *Journal of Dental Research* **2006**, 85, (4), 359-363.
9. N. Batina; V. Renugopalakrishnan; P. N. C. Lavin; J. C. H. Guerrero; M. Morales; R. Garduno-Juarez, *Journal of Biomaterials Science-Polymer Edition* **2002**, 13, (3), 337-348.
10. G. Gualtieri; S. Colacicchi; R. Sgattoni; M. Giannoni, *Research on Chemical Intermediates* **2001**, 27, (9), 945-956.
11. L. J. Wang; R. K. Tang; T. Bonstein; C. A. Orme; P. J. Bush; G. H. Nancollas, *Journal of Physical Chemistry B* **2005**, 109, (2), 999-1005.
12. C. F. Li; S. Risnes, *Archives of Oral Biology* **2004**, 49, (1), 45-52.
13. G. H. Dibdin, *Journal of Dental Research* **1990**, 69, (6), 1324-1331.
14. H. C. Margolis; Y. P. Zhang; C. Y. Lee; R. L. Kent; E. C. Moreno, *Journal of Dental Research* **1999**, 78, (7), 1326-1335.
15. P. Anderson; F. R. G. Bollet-Quivogne; S. E. P. Dowker; J. C. Elliott, *Archives of Oral Biology* **2004**, 49, (3), 199-207.
16. P. Anderson; J. C. Elliott, *Caries Research* **2000**, 34, (1), 33-40.
17. M. Maltz; S. C. Scherer; C. C. F. Parolo; J. J. Jardim, *Caries Research* **2006**, 40, (3), 251-255.
18. T. Aoba, *Oral Diseases* **2004**, 10, (5), 249-257.
19. A. J. Gwinnett, *Journal of Dental Research* **1966**, 45, (3), 870-873.
20. J. Thewlis, *Proceedings of the Royal Society of London. Series B, Biological Sciences (1934-1990)* **1939**, 127, (847), 211-223.
21. R. J. M. Lynch; J. M. ten Cate, *Caries Research* **2006**, 40, (6), 530-535.
22. C. T. K. Alex; C.-S. Lin-P'ing; H. Mark; L. Lorenzo; G. S. Michael; C. S. D. Cecilia; W. Peter; C. Blaine, in: SPIE: 2005; Vol. 10, p 031118.
23. K. Tanaka; Y. Iijima, *Journal of Dentistry* **2001**, 29, (6), 421-426.
24. H. El Feki; J. M. Savariault; A. Ben Salah; M. Jemal, *Solid State Sciences* **2000**, 2, (5), 577-586.
25. J. D. Pasteris; B. Wopenka; J. J. Freeman; K. Rogers; E. Valsami-Jones; J. A. M. van der Houwen; M. J. Silva, *Biomaterials* **2004**, 25, (2), 229-238.
26. J. P. Simmer; J. C. Hu, *Journal of Dental Education* **2001**, 65, (9), 896-905.
27. P. Tramini; B. Pelissier; J. Valcarcel; B. Bonnet; L. Maury, *Caries Research* **2000**, 34, (3), 233-240.

28. J. Palamara; P. P. Phakey; W. A. Rachinger; H. J. Orams, *Advances Dental Research* **1989**, 3, (2), 249-257.
29. L. Breschi; P. Gobbi; G. Mazzotti; T. H. Ellis; E. Sacher; I. Stangel, *Journal of Biomedical Materials Research* **1999**, 46, (3), 315-323.
30. A. I. Darling, *Annals of the Royal College of Surgeons of England* **1961**, 29, 354-369.
31. E. C. Moreno; R. T. Zahradnik, *Journal of Dental Research* **1974**, 53, (2), 226-235.
32. S. Cazalbou; C. Combes; D. Eichert; C. Rey, *Journal of Materials Chemistry* **2004**, 14, (14), 2148-2153.
33. E. B. Hanlon; R. Manoharan; T. W. Koo; K. E. Shafer; J. T. Motz; M. Fitzmaurice; J. R. Kramer; I. Itzkan; R. R. Dasari; M. S. Feld, in: 2000; p R1.
34. Y. Chiang; D. P. Birnie; W. D. Kingery, *Physical ceramics : principles for ceramic science and engineering*. J. Wiley: New York, 1997; p xiv, 522 p.
35. M. E. Dickinson, *Surface variations affecting human dental enamel studied using nanomechanical and chemical analysis. Ph.D. Thesis, Rutgers University*: 2005.
36. M. E. Dickinson; K. V. Wolf; A. B. Mann, *Archives of Oral Biology* **2007**, 52, (8), 753-760.
37. Derek G. Leaist; Paul Anderson; J. C. Elliott, *J. Chem. Soc., Faraday Trans.* **1990**, 86, 3093 - 3095.
38. A. Boyde, *Operative dentistry* **1976**, 1, (1), 13-28.
39. J. C. Elliott, *Ciba Foundation symposium* **1997**, 205, 54-67; discussion 67-72.
40. C. Robinson; R. C. Shore; S. J. Brookes; S. Strafford; S. R. Wood; J. Kirkham, *Critical Reviews in Oral Biology Medicine* **2000**, 11, (4), 481-495.
41. A. A. Baig; J. L. Fox; R. A. Young; Z. Wang; J. Hsu; W. I. Higuchi; A. Chhettry; H. Zhuang; M. Otsuka, *Calcified Tissue International* **1999**, 64, (5), 437-449.
42. H. Rietveld, in: *Journal of Applied Crystallography*, 1969; Vol. 2, pp 65-71.
43. D. Deutsch; J. CatalanoSherman; L. Dafni; S. David; A. Palmon, *Connective Tissue Research* **1995**, 32, (1-4), 97-107.
44. C. Robinson; S. J. Brookes; R. C. Shore; J. Kirkham, *European Journal of Oral Sciences* **1998**, 106, 282-291.
45. S. Risnes, *Journal of Human Evolution* **1998**, 35, (4-5), 331-350.
46. H. F. Chen; B. H. Clarkson; K. Sun; J. F. Mansfield, *Journal of Colloid and Interface Science* **2005**, 288, (1), 97-103.
47. M. T. Kirchner; H. G. M. Edwards; D. Lucy; A. M. Pollard, *Journal of Raman Spectroscopy* **1997**, 28, (2-3), 171-178.
48. A. I. Darling, *Journal of Dental Research* **1963**, 42, (1), 488-496.
49. A. Carden; M. D. Morris, *Journal of Biomedical Optics* **2000**, 5, (3), 259-268.
50. J. A. Timlin; A. Carden; M. D. Morris, *Applied Spectroscopy* **1999**, 53, 1429-1435.
51. G. Penel; G. Leroy; C. Rey; E. Bres, *Calcified Tissue International* **1998**, 63, (6), 475-481.
52. G. Leroy; G. Penel; N. Leroy; Br; E. s, *Applied Spectroscopy* **2002**, 56, 1030-1034.

53. R. P. Rusin; G. Fischman; American Ceramic Society. Meeting, *Bioceramics : materials and applications II*. American Ceramic Society: Westerville, Ohio, 1996; p vii, 136 p.
54. G. Fischman; A. Clare; L. L. Hench; American Ceramic Society. Meeting, *Bioceramics : materials and applications*. American Ceramic Society: Westerville, Ohio, 1995; p vii, 329 p.
55. R. P. Shellis; A. R. Lee; R. M. Wilson, *Journal of Colloid and Interface Science* **1999**, 218, (2), 351-358.
56. A. Ito; K. Maekawa; S. Tsutsumi; F. Ikazaki; T. Tateishi, *Journal of Biomedical Materials Research* **1997**, 36, (4), 522-528.
57. H. Fong; S. N. White; M. L. Paine; W. Luo; M. L. Snead; M. Sarikaya, *Journal of Bone and Mineral Research* **2003**, 18, (11), 2052-2059.

APPENDICES

APPENDIX 1

PREPARATION OF METHYL CELLULOSE GEL FOR DEMINERALISATION SOLUTION

Equipment:

Methyl Cellulose (Sigma Aldrich)

500 ml glass beaker

60 ml glass sterilin

Distilled Water

Magnetic Stirrer with Hotplate

Magnetic Stirrer Flea

Thermometer

Balance

Method:

16 grams of Methyl Cellulose powder was weighed into sterilin. 200 ml deionised water was brought to boil in the beaker and allowed to cool slightly. Upon cooling to 70 °C, a stirrer flea was added to the beaker and Methyl Cellulose powder stirred in until the solution was thoroughly blended. Care was taken to ensure that the temperature did not fall below 50 °C whilst adding and mixing powder, then the solution was allowed to cool to 40 °C.

This solution was then immediately poured over the wax mounted teeth.

APPENDIX II

PRODUCTION OF LACTIC ACID SOLUTION FOR DIMINERALISATION
SOLUTION

Equipment:

BDH Lactic acid solution

60 ml Sterilin

Distilled Water

Glass beaker

1 litre conical flask

Funnel

Stirrer Flea

PH meter

Potassium Hydroxide flakes

Volumetric Flask

Method:

10.58 grams of BDH lactic acid solution was weighed into a 60 ml sterilin and transferred to a 1 litre conical flask using a large funnel.

400 ml of distilled water was measured into a glass beaker and poured into the conical flask using the funnel to ensure no acid was remaining on the surface.

In a fume cupboard, the conical flask was placed on a magnetic hotplate/stirrer and stirred using a magnetic flea.

Once the solution reached boiling point, it was left on low heat for 1 hour to allow acid to hydrolyse, then removed from heat and allowed to cool. Whilst stirring, a further 500 ml of distilled water solution was added and the whole solution titrated using potassium hydroxide to a pH of 4.6, or 5.5 or 6.3.

The final solution was made up to 1 litre with distilled water and stored in the refrigerator at 5 °C until needed.

APPENDIX III POLISHING OF BIOGLASS SAMPLES

The glass pieces were embedded in epoxy and polished at grit sizes 320 (150 rpm, 20 mins) , 600/1200 (150 rpm, 30 mins), 2400 (200 rpm , 15 mins), 4000 (300 rpm , 15 mins). Shown below in figure 1 and figure 2 are the images of sections of Bioglass observed under an optical microscope with magnification 20x, and 50x.

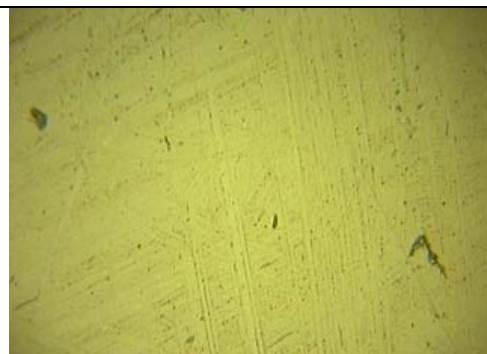


Figure 9.1: Polished Bioglass section 20x

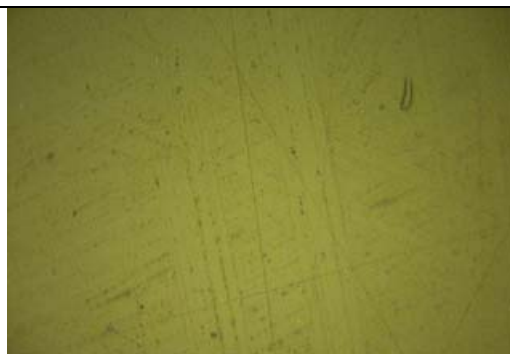


Figure 9.2: Polished Bioglass section 50x